mathematics

MDPI

Article

A Modified Gradient Search Rule Based on the Quasi-Newton Method and a New Local Search Technique to Improve the Gradient-Based Algorithm: Solar Photovoltaic Parameter Extraction

Bushra Shakir Mahmood [1], Nazar K. Hussein [1], Mansourah Aljohani [2] and Mohammed Qaraad [3,4,*]

[1] Department of Mathematics, College of Computer Sciences and Mathematics, Tikrit University, Tikrit 34001, Iraq; bushra.s.mahmoud35379@st.tu.edu.iq (B.S.M.); nazar.dikhil@tu.edu.iq (N.K.H.)
[2] College of Computer Science and Engineering, Taibah University, Yanbu 46421, Saudi Arabia; mjohni@taibahu.edu.sa or aljohani.mk@gmail.com
[3] Computer Science Department, Faculty of Science, Abdelmalek Essaadi University, Tetouan 93000, Morocco
[4] Department of Computer Science, Faculty of Science, Amran University, Amran 9677, Yemen
* Correspondence: mohammedalimohammed.qaraad@uae.ac.ma

Abstract: Harnessing solar energy efficiently via photovoltaic (PV) technology is pivotal for future sustainable energy. Accurate modeling of PV cells entails an optimization problem due to the multimodal and nonlinear characteristics of the cells. This study introduces the Multi-strategy Gradient-Based Algorithm (MAGBO) for the precise parameter estimation of solar PV systems. MAGBO incorporates a modified gradient search rule (MGSR) inspired by the quasi-Newton approach, a novel refresh operator (NRO) for improved solution quality, and a crossover mechanism balancing exploration and exploitation. Validated through CEC2021 test functions, MAGBO excelled in global optimization. To further validate and underscore the reliability of MAGBO, we utilized data from the PVM 752 GaAs thin-film cell and the STP6-40/36 module. The simulation parameters were discerned using 44 I-V pairs from the PVM 752 cell and diverse data from the STP6-40/36 module tested under different conditions. Consistency between simulated and observed I-V and P-V curves for the STM6-40/36 and PVM 752 models validated MAGBO's accuracy. In application, MAGBO attained an RMSE of 9.8×10^{-4} for double-diode and single-diode modules. For Photowatt-PWP, STM6-40/36, and PVM 752 models, RMSEs were 2.4×10^{-3}, 1.7×10^{-3}, and 1.7×10^{-3}, respectively. Against prevalent methods, MAGBO exhibited unparalleled precision and reliability, advocating its superior utility for intricate PV data analysis.

Keywords: metaheuristic; gradient-based optimizer; photovoltaic parameter estimation; global optimization

MSC: 68T20

Citation: Mahmood, B.S.; Hussein, N.K.; Aljohani, M.; Qaraad, M. A Modified Gradient Search Rule Based on the Quasi-Newton Method and a New Local Search Technique to Improve the Gradient-Based Algorithm: Solar Photovoltaic Parameter Extraction. *Mathematics* **2023**, *11*, 4200. https://doi.org/10.3390/math11194200

Academic Editor: Ioannis G. Tsoulos

Received: 28 August 2023
Revised: 26 September 2023
Accepted: 27 September 2023
Published: 8 October 2023

1. Introduction

In recent decades, interest in renewable energy sources has become very large due to environmental concerns resulting from fossil fuel pollution, global warming, solid waste, the dangers of burning coal, and the instability of fossil fuel prices. Many alternative energy sources have been found to avoid this, such as wind, water, solar energy, and others. Moreover, solar energy is considered one of the most important energy sources for generating electricity due to its high availability, safe and pollution-free manufacturing methods, and noise-free manufacturing methods. In addition, the price of solar cells has decreased in recent years.

The popularity of solar photovoltaic (PV) systems has increased nowadays because of their use of solar cells [1]. These technologies' ability to convert solar energy into electricity is impressive. In order to regulate and optimize PV systems, it is crucial to build a precise

model that incorporates observed current-voltage data, as this enables the evaluation of the PV array's actual behavior. Several mathematical models have been developed to shed light on the performance and nonlinear features of PV systems [2], with single-diode and double-diode setups being the most common and commonly used.

The reliability of the parameters is intrinsically tied to the accuracy of the photovoltaic (PV) models. However, environmental variables such as temperature, global irradiation, material flaws, and shifting operational conditions make it difficult to consistently achieve these requirements. Therefore, accurate models that outline the complex relationship between current and voltage are required for the optimization and control of PV systems [3]. In recent years, numerous parameter identification approaches have been developed to meet this pressing requirement [4].

Recently, numerous strategies for finding the parameters of photovoltaic (PV) models have been put forward as potential solutions. They can generally be divided into the following three categories: (1) analytical methods, which are mainly based on the short circuit point, open circuit point, and maximum power point; these methods are fast, simple, and unique, but they are not accurate [5–11]. (2) Deterministic methods. These methods are sensitive to the initial values and require a level of calculus and convexity. However, they are still not precise enough in the same manner as Newton's approach [12], the Newton–Raphson approach [13], or the method of the nonlinear algorithm [14]. (3) Meta-heuristic methods are a promising and powerful solution to extract the parameters of the photovoltaic model, and because they are easy to implement and most of them are inspired by the phenomena of nature, they do not need convexity conditions or the derivation of the objective function. Despite developing a set of optimization algorithms, they fail to provide satisfactory results, so meta-heuristic algorithms have been used to solve difficult and complex problems [15].

Consequently, many metaheuristic algorithms have been developed and applied in many fields and to extract the parameters of photoelectric models. The parameters of the diode model of a polycrystalline solar module cell were extracted using the moth optimization algorithm [16], the genetic algorithm (GA), which was derived from Darwin's development theory [17], particle swarm optimization (PSO) [18], simulated annealing algorithm (SA) [19], artificial bee colony (ABC) [20], anarchic asexual reproduction (CARO) [21], multiple learning backtracking search (MLBSA) [22], cuckoo search algorithm (CS) [23], biogeography optimization (BBO) [24], MBO algorithm [25], sunflower optimization algorithm (SFO) [26], coyote optimization algorithm (COA) [27], Bacterial Foraging Optimization (BFO) [28], Harris haws optimization (HHO) [29], and modified flower algorithm (MFA) [30].

As a direct consequence of this, efforts are currently being undertaken to create more effective optimization algorithms to calculate the parameters of solar photovoltaic cells [31,32]. In the next parts, an in-depth discussion on optimizing photovoltaic systems will be held, focusing on previously developed and evaluated methods.

The algorithms discussed earlier have been applied to various topics, and their results have been found to be satisfactory. However, according to the No Free Lunch theorem [33], there is not yet a superior method of optimization in all circumstances. Furthermore, many optimization methods have benefits and drawbacks that are comparable to one another [34,35]. These approaches, for instance, have a substantial benefit in that they can handle a diverse range of systems with nonlinear fitness functions and restrictions [36]. This is just one example. The primary drawbacks include difficulty adjusting their parameters, the potential for early convergence, the inability to find global optimal solutions, the lack of diversity, and the instability in balancing exploration and exploitation in the solution space [37,38]. These drawbacks can be overcome, however, by using alternative approaches. These methods, if developed with care, have the potential to provide extraordinary performance and versatility for solving difficult optimization problems in the real world [39,40].

As per the No Free Lunch theory, existing optimization algorithms have limitations and weaknesses [41–44] and may not be suitable for all types of problems. Thus, there is still potential for improvement in algorithm efficiency. Recent studies have focused on developing new ways to improve fundamental optimization procedures by integrating a variety of initial design strategies [45–47], hybridizing optimization procedures [48,49], and altering search patterns [50–54]. The Gradient-based Algorithm (GBO), a population-based optimization technique, is an exciting new discovery made very recently. This technique has demonstrated that it is effective and precise in its optimization outcomes. During the phase of exploration and exploitation, GBO uses the information that is available to find optimal or near-optimal solutions by randomly selecting two solutions from the population to predict future relocation and direction based on the best search options. This helps GBO find the best possible options. However, it has been discovered that the new optimization method of GBO has significant drawbacks in high-dimensional and multimodal problems. These drawbacks include getting stuck in local solutions as the size of the search space increases and having poor convergence performance in difficult problems [55,56].

Additionally, the characteristics of the objective function have the potential to have a negative impact on the performance of the algorithm in specific contexts. Particularly when dealing with issues that include many modes of communication, the search method may be hampered. It is well known that the objective function for Solar Photovoltaic Parameter Estimation problems is multimodal and nonlinear with multiple local minimums. Because of this, it is challenging to develop new robust optimization techniques that can produce more accurate and faster convergence results.

This study aims to find the best values for the parameters of Photovoltaic systems. To achieve this, this study proposes a modified gradient search rule (MGSR) based on the quasi-Newton method, derives the MGSR factor that controls vector motion to improve its local and global capabilities, and enhances exploration to improve the search in the selected area. In addition, a new refresh operator (NRO) has been proposed to enhance the algorithm's solution quality and exploration abilities, as well as a strong crossover mechanism to balance exploitation and increase population diversity. The proposed method, MAGBO, is tested for its performance on CEC2021 benchmark functions and a complex Photovoltaic system. The results are compared with various optimization methods such as Gradient-based Algorithm (GBO), Gradient-based optimization with ranking mechanisms (EGBO), Slime mould algorithm (SMA), Self-adaptive differential evolution algorithm (SADE), Equilibrium optimizer (EO), new self-organizing hierarchical PSO with jumping time-varying acceleration coefficients (HPSO_TVAC), comprehensive learning particle swarm optimizer (CL-PSO), Improved Jaya Algorithm (IJAYA), performance-guided JAYA algorithm (PGJAYA), and multiple learning backtracking search MLBSAs, which shows that MAGBO outperforms the other methods in this context. The Wilcoxon rank-sum and Friedman statistical tests are used to confirm the validity of MAGBO.

The heart of this research revolves around the advanced development and meticulous validation of the MAGBO technique, tailored for photovoltaic system parameter identification. Specifically:

- Modified Gradient Search Rule (MGSR): utilizes the quasi-Newton method to bolster both local and global optimization.
- Crossover Mechanism: introduced to ensure greater agent diversity and prevent premature convergence.
- Novel Refresh Operator (NRO): enhances solution quality and strategic exploration, balancing exploration and exploitation.
- Rigorous Validation: comprehensive evaluation of various SDMs, DDMs, and PV modules, showcasing MAGBO's superiority over older methods.

To organize the remainder of this paper, the second section focuses on MAGBO's related work. The original GBO and problem statement are presented in Section 3. Section 4 explains the details of the proposed MAGBO. In Section 5, experimental results

and comparisons are presented. Section 6 discusses the problematic constraints and difficulties, and finally, Section 7 concludes with the conclusions and future work.

2. Related Work

In addition to analytical and deterministic methods, heuristic methods have also been proposed for determining the parameters of PV models. Heuristic methods are typically based on the principles of human reasoning and problem-solving, and they can be used to find approximate solutions to complex problems. Some of the most popular heuristic methods for determining the parameters of PV models include genetic algorithms (GA), artificial bee colonies (ABC), particle swarm optimization (PSO), ant lion optimizer (ALO), biogeography-based optimization (BBO), whale optimization algorithm (WOA), JAYA algorithm, differential evolution (DE), teaching-learning-based optimization (TLBO), harmony search (HS), flower pollination algorithm (FPA), and moth flame optimization algorithm (MFO). Each of these methods has its advantages and disadvantages, and the best method for a particular problem will depend on the specific characteristics of the problem [22,49,57–59]. Even though it has been shown that these methods are effective and consistent, most heuristic algorithms still struggle with locating the best possible solution for the whole problem. Estimating parameters in PV models is difficult since the objective function is multimodal, meaning it has numerous local minima. This makes parameter estimation a complex task. Because of this, locating the global minimum, which represents the optimal course of action, can be challenging. In addition, numerous heuristic methods call for particular control parameters, in addition to population size and the number of generations, which substantially influence the overall performance. Incorrect tuning can result in increased computation expenses as well as software that is insensitive to user input.

As a consequence of this, the issue of establishing a trustworthy heuristic approach for predicting PV model parameters continues to be challenging. The most recent and applicable research approaches are outlined in Table 1, which provides an overview of them. This study aims to give both a potential solution to the issue by way of an updated version of the Mas algorithm, which is a method for estimating the parameters of solar PV models, and to suggest a new version of the algorithm.

Table 1. The methodologies of the recent modification/hybridization of GBO.

Algorithm and Ref.	Methodology	Type of Improvement	Problem Formulation	Statistical Test
Modified Gradient-Based Optimizer (MGBO) [60]	The strategy is to adjust the value of the direction of movement (DM) by introducing a new number D that ranges from 1 to 2 and goes up in increments of 1.	Modification	Three Photovoltaics module (single, double-diode), and PV module.	none
Improved gradient-based optimizer (IBGO) [61]	Two different approaches have been suggested as ways to enhance the functionality of meta-heuristic algorithms. The first tactic employs adaptive weights to move closer to the optimal solution and stay out of local optima during the various phases of the method. The second tactic involves substituting chaotic behavior for the algorithm's inherent unpredictability to boost the method's convergence speed and accuracy.	Modification	Three Photovoltaics module (single, double-diode), and PV module.	none
Opposition decided gradient-based optimizer (OBGBO) [62]	OBGBO is an enhancement over GBO, which employs an opposition-based process to produce more precise answers. OBGBO uses the same technique to generate solutions, but it does so in a different way.	Modification	Three Photovoltaics module (single, double-diode), and PV module.	none
Random learning gradient based optimization (RLGBO) [63]	To solve the issue of the GBO being stuck in local optima and to make the convergence process faster and more accurate, a new learning mechanism based on randomization was added to the original version of the GBO. The random learning mechanism allows individuals to maintain constant communication with one another, ultimately resulting in improved performance.	Modification	three various PV models (KC200GT, ST40, and SM55)	Wilcoxon ranked test

Table 1. *Cont.*

Algorithm and Ref.	Methodology	Type of Improvement	Problem Formulation	Statistical Test
Sine cosine differential gradient based optimizer (SDGBO) [64]	The suggested method utilizes the mutation crossover of the differential evolution algorithm in conjunction with the sine cosine method. With either the crossover operator or the sine cosine approach, the new search agent is encouraged to determine the absolute worst place to settle. By doing so, the algorithm is freed from the confines of whatever local optimums it might have been experiencing.	Hybridization	Four various PV models, and (KC200GT)	Wilcoxon ranked test
Developed Version of Eagle Strategy Gradient-Based Optimizer (ESCGBO) [65]	Estimating the parameters of static and dynamic photovoltaic models led to developing an updated version of the GBO algorithm known as ESCGBO. The ESCGBO employs a strategy known as the chaotic eagle. The authors carried out assessments to establish that ESCGBO is successful on both a macro and micro level.	Hybridization	23 benchmark functions and three various PV models	None
Improved moth flame algorithms (IMFOL) [66]	IMFOL stands for Improved Moth Flame with Local escape operators, which is the name of the algorithm that has been proposed. The MFO algorithm is enhanced by adding the Local Escape Operators method, which ultimately leads to improved performance in terms of accuracy and efficiency. Additionally, the LEO strategy broadens the demographic range of the population and improves the MFO algorithm's ability to explore uncharted territories efficiently.	Hybridization	five various PV models	None

3. Preliminaries

Within this section, the algorithm for gradient-based optimization and the problem statement are broken down into their component parts.

3.1. Principles of Gradient-Based Optimizer (GBO)

The GBO algorithm [17] is one of the effective methods for solving complex optimization problems due to its ability to explore, exploit, converge, and move away from the local optimal solution. The method component has two main factors, GSR search base and LEO local escape factor.

3.1.1. Initialization

The initial population in GBO is a matrix with N rows and d columns, where N is the size of the population and d is the number of variables of the problem. The initial population is randomly generated using the following equation:

$$X_n = Lb + rand \times (Ub - Lb) \tag{1}$$

where X_n represents the vector member, Lb represents the lower-bounded, Ub represents the upper-bounded of the problem, and $rand$ denotes a random number in the range (0, 1).

3.1.2. Gradient Search Rule (GSR)

The first factor of GBO controls the vector movement to improve the search in the field and achieve better locations in the solution area. The GSR based on Newton's method was proposed according to [67]. Therefore, the GSR is defined as:

$$GSR = rand \times \rho_1 \times \frac{2\Delta x \times x_n}{y_{an}^m - y_{bn}^m + \epsilon} \tag{2}$$

y_{an}^m and y_{bn}^m are employed to search inside a population to enhance diversity and robustness. Equations (3) and (4) display the y_{an}^m and y_{bn}^m formula.

$$y_{an}^m = rand \times \left(\frac{(u_{n+1} - x_n)}{2} + rand \times \Delta x \right) \tag{3}$$

$$y_{bn}^{m} = rand \times \left(\frac{(\ u_{n+1} - x_n)}{2} - rand \times \Delta x \right) \tag{4}$$

$$u_{n+1} = x_n^m \ - rand \times \rho_1 \times \frac{2\Delta x \times x_n^m}{x_{worst} - x_{best} + \epsilon} + DM \Big) \tag{5}$$

where *rand* is a random number in the interval of [0, 1], u_{n+1} signifies the new solution produced by the GBO, x_{worst} and x_{best} represent the worst and best solutions found throughout the optimization process, respectively, and ϵ denotes a small number in the [0, 0.1] range.

$$\rho_1 = 2 \times rand \times \alpha - \alpha \tag{6}$$

$$\alpha = \left| \beta \times \sin\left(\frac{3\pi}{2} \right) + \sin\left(\beta \times \frac{3\pi}{2} \right) \right| \tag{7}$$

$$\beta = \beta_{\min} + (\ \beta_{\max} - \beta_{\min}\ ) \times \left(1 - \left(\frac{4}{3} \right)^3 \right)^2 \tag{8}$$

where parameter ρ_1 changes based on the sine function to balance exploration and exploitation, $\beta_{\min}$ and $\beta_{\max}$ are 0.2 and 1.2, respectively, and Δx the difference between the vectors, which are define as:

$$\Delta x = rand \times |\tau| \tag{9}$$

$$\tau = \frac{(x_{best} - x_{d1}^m) + \delta}{2} \tag{10}$$

$$\delta = 2 \times rand \times \left(\left| \frac{x_{d1}^m + x_{d2}^m + x_{d3}^m + x_{d4}^m}{4} - x_n^m \right| \right) \tag{11}$$

where r_1, r_2, r_3, and r_4 ($r_1 \neq r_2 \neq r_3 \neq r_4 \neq n$) are integers randomly chosen from $\{1, 2, \ldots, \mathrm{N}\}$, and τ denotes the step size.

Adding the (DM) limit will improve the performance of the algorithm by making better exploitation in the vicinity of the point x_n, since (DM) will make the movement of the vector x_n be in the direction of $(x_{best} - x_n)$. Therefore, this process creates a suitable local search tendency to promote the convergence speed of the GBO algorithm. The proposed DM is formulated as follows:

$$DM = rand \times \rho_2 \times (x_{best} - x_n) \tag{12}$$

$$\rho_2 = 2 \times rand \times \alpha - \alpha \tag{13}$$

3.1.3. Generate New Solutions

The GSR and DM techniques update the population's position. The three new species $X1_n^m$, $X2_n^m$, and $X3_n^m$ are used to determine the final population location update in order to better balance the global search and local search. They are defined by the formulas in the following equations:

$$X1_n^m \ = x_n^m \ - GSR + DM \tag{14}$$

$$X1_n^m \ = x_n^m \ - rand \times \rho_1 \times \frac{2\Delta x \times x_n^m}{y_{an}^m - y_{bn}^m + \epsilon} + rand \times \rho_2 \times (x_{best} - x_n^m) \tag{15}$$

where m is the current of iteration. The problem's parameters support the exploration process given an appropriate step size. By replacing the current position with the best position, a new value will be generated that can be generated using the following equation:

$$X2_n^m = x_{best} - rand \times \rho_1 \times \frac{2\Delta x \times x_n^m}{y_{an}^m - y_{bn}^m + \epsilon} + rand \times \rho_2 \times \left(x_{r_1}^m - x_{r_2}^m\right) \quad (16)$$

where r_1, r_2 are two random numbers. Accordingly, based on the positions $X1_n^m$, $X2_n^m$, and the current position x_n^m, the new solution at the next iteration can be defined as:

$$X_n^{m+1} = r_i \times \left(r_j \times X1_n^m + \left(1 - r_j\right) \times X2_n^m\right) + (1 - r_i) \times X3_n^m \quad (17)$$

$$X3_n^m = x_n^m - \rho_1 \times (X2_n^m - X1_n^m) \quad (18)$$

where r_i and r_j are two random numbers in [0, 1].

3.1.4. Local Escaping Operator (LEO)

The GBO algorithm suggests a LEO method to boost the effectiveness of handling complicated issues. With the help of this operator, the position of X_n^{m+1} is improved, the population's diversity is increased, and the algorithm is assisted in leaving the local optimum. LEO starts by producing a random number, *rand* as a random number in the interval $[0, 1]$. Equation (19) displays the LEO updating formula when *rand* is bigger than 0.5. Equation (20) displays the LEO updating formula when *rand* is smaller than 0.5.

$$X_{LEO}^m = X_n^{m+1} + q_1 \times (\sigma_1 \times x_{best} - \sigma_2 \times x_s^m) + q_2 \times \rho_1 \times (\sigma_3 \times (X2_n^m - X1_n^m) + \sigma_2 \times (x_{r1}^m - x_{r2}^m))/2 \quad (19)$$

$$X_{LEO}^m = x_{best} + q_1 \times (\sigma_1 \times x_{best} - \sigma_2 \times x_s^m) + q_2 \times \rho_1 \times (\sigma_3 \times (X2_n^m - X1_n^m) + \sigma_2 \times (x_{r1}^m - x_{r2}^m))/2 \quad (20)$$

where q_1 and q_2 are uniform random numbers in the interval $[-1, 1]$ and σ_2 is a random number from a normal distribution with mean of 0 and standard deviation of 1.

$$\sigma_1 = \begin{cases} 2 \times rand \; if \; \varphi_1 < 0.5 \\ 1 \; otherwise \end{cases} \quad (21)$$

$$\sigma_2 = \begin{cases} rand \; if \; \varphi_1 < 0.5 \\ 1 \; otherwise \end{cases} \quad (22)$$

$$\sigma_3 = \begin{cases} rand \; if \; \varphi_1 < 0.5 \\ 1 \; otherwise \end{cases} \quad (23)$$

where *rand* is a random number in the interval of [0, 1] and φ_1 is a number in the interval [0, 1].

To determine the solution x_s^m in Equations (19) and (20), the following scheme is defined.

$$x_s^m = \begin{cases} x_l \; if \; \varphi_2 < 0.5 \\ x_l^m \; otherwise \end{cases} \quad (24)$$

$$x_l = Lb + rand \times (Ub - Lb) \quad (25)$$

where x_l is a new solution and is a randomly selected solution of the population ($l \in \{1, 2, \ldots, N\}$) and φ_2 and *rand* are random numbers in the interval of [0, 1].

3.2. Problem Statement

This section will describe two PV models, namely SDM and DDM, as SDM depends on the PV module (SMM) and the objective function.

3.2.1. Single-Diode Model

The SDM model is widely used because of its simple structure and high accuracy in extracting and explaining the features of solar cells [68,69]. The SDM's equivalent circuit for the load current is depicted in Figure 1. The combination of the current source, the diode, and the shunt resistor determines the current through the load. This circuit shows

both the leakage current and the electrical resistance of the battery [70]. Here is how you can write down the equation for SDM results:

$$I = I_{ph} - I_d - I_{sh} \tag{26}$$

where I stands for output current, I_{ph} is the photo-induced current, I_d is the diode current, I_{sh} is the shunt resistor current, and as follows:

$$I_d = I_0 \left[\exp\left(\frac{V + IR_s}{\alpha V_t} \right) - 1 \right] \tag{27}$$

$$I_{sh} = \frac{V + IR_S}{R_{sh}} \tag{28}$$

where I_0 represents the diode reverse saturation current, α represents the ideal factor, R_s represents the series resistance, R_{sh} represents the shunt resistance, V represents the output voltage of the cell, and V_t is the thermal conductivity potential and is given as:

$$V_t = \frac{k \times T}{q} \tag{29}$$

where T represents the crossroads temperature in Kelvin, k refers to the Boltzmann constant ($1.3806503 \times 10^{-23}$ J/K), and q is the electron charge ($1.60217646 \times 10^{-19}$C).

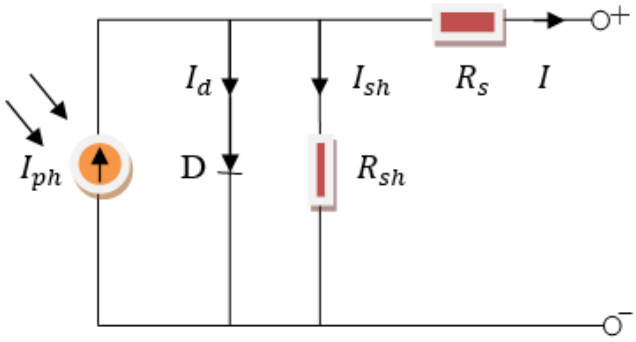

Figure 1. Equivalent circuit diagram of the SDM model.

Substituting Equations (27) and (28) into Equation (17) gives:

$$I = I_{ph} - I_0 \left[\exp\left(\frac{V + IR_s}{\alpha V_t} \right) - 1 \right] - \frac{V + IR_S}{R_{sh}} \tag{30}$$

3.2.2. Double-Diode Model

The SDM single-diode model does not consider current recombination loss in the shading layer, which is a limitation of the model. To address this problem, researchers proposed the DDM dual diode model [71]. The two primary diodes work in parallel with the photovoltaic and shunt currents. These diodes can also be described as the first diode acting as a rectifier and the second as a designer to mimic the recombination of current charges and other factors that cannot be controlled. Figure 2 shows the DDM equivalent circuit, and the output equation can be formulated as follows [72]:

$$I = I_{ph} - I_{d1} - I_{d2} - I_{sh} \tag{31}$$

$$I_{d1} = I_{01} \left[\exp\left(\frac{V + IR_s}{\alpha_1 V_t} \right) - 1 \right] \tag{32}$$

$$I_{d2} = I_{02}\left[\exp\left(\frac{V + IR_s}{\alpha_2 V_t}\right) - 1\right] \tag{33}$$

where I_{d1} indicates the first diode current, I_{d2} is the second diode current, I_{01} indicates the diffusion current, I_{02} denotes the saturation current, and α_1, α_2 are the first and second diode ideality factor, sequentially. Substituting Equations (32) and (33) into Equation (34), we obtain:

$$I = I_{ph} - I_{01}\left[\exp\left(\frac{V + IR_s}{\alpha_1 V_t}\right) - 1\right] - I_{02}\left[\exp\left(\frac{V + IR_s}{\alpha_2 V_t}\right) - 1\right] - \frac{V + IR_S}{R_{sh}} \tag{34}$$

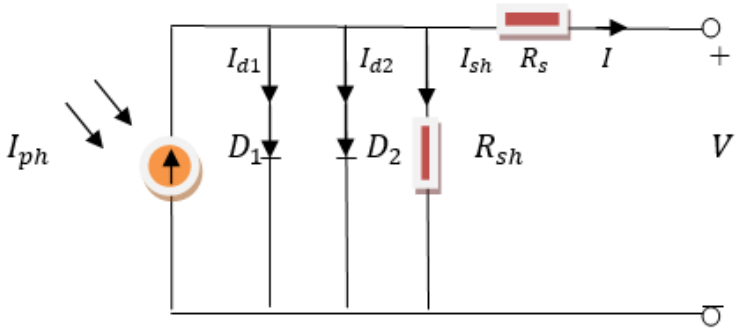

Figure 2. Equivalent circuit diagram of the DDM model.

3.3. Photovoltaic Module

Figure 3 shows that we can obtain a relationship between voltage and current by using several diodes connected in series or parallel. The photoelectric model can be formulated based on SMM with the following formula [72]:

$$I = I_{ph}N_p - I_o N_p\left[\exp\left(\frac{V + IR_s N_s}{\alpha N_s V_t}\right) - 1\right] - \frac{V + IR_s N_s / N_p}{R_{sh} N_s / N_p} \tag{35}$$

where N_p denoted to the number of solar cells connected in parallel and N_s refers to the number of solar cells connected in series. In SMM we used the series connection so that N_p equals one, and this can be expressed by the equation:

$$I = I_{ph} - I_o\left[\exp\left(\frac{V + IR_s N_s}{\alpha N_s V_t}\right) - 1\right] - \frac{V + IR_s N_s}{R_{sh} N_s} \tag{36}$$

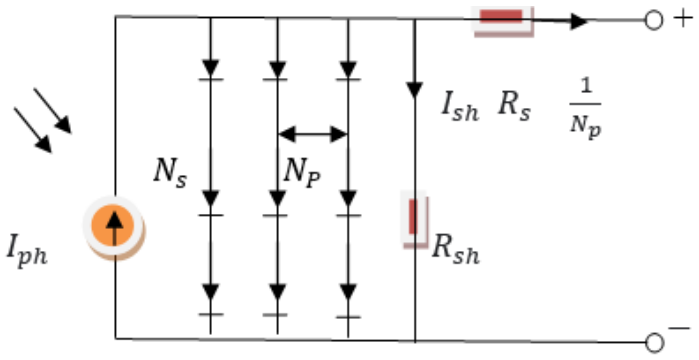

Figure 3. Equivalent circuit diagram of the SMM model.

Parameters $(I_{ph},\ I_o, R_s, R_{sh},\ \alpha)$ are unknown and are to be found by differentiation.

3.4. The Cost Functions

Parameter problems are often transformed into optimization problems by using optimization algorithms [73,74]. Researchers [75] used the Root Mean Square Error (RMSE) as the target function, as in the equation below:

$$RMSE = \sqrt{\frac{1}{M}\sum_{m=1}^{M} f(V_m, I_m, x)^2} \tag{37}$$

The objective function for various photovoltaic models is shown in Table 2. M is the number of estimated I-V datasets and x is considered as a vector for measuring the extracted parameters.

Table 2. Objective function and variables of different PV models.

PV Model	Objective Function	Parameters
	$f(V, I, x)$	x
SDM	$I_{ph} - I_0\left[\exp\left(\frac{V+IR_s}{\alpha V_t}\right) - 1\right] - \frac{V+IR_S}{R_{sh}} - I$	$\left(I_{ph},\ I_o, R_s, R_{sh},\ \alpha\right)$
DDM	$I = I_{ph} - I_{01}\left[\exp\left(\frac{V+IR_s}{\alpha_1 V_t}\right) - 1\right] - I_{02}\left[\exp\left(\frac{V+IR_s}{\alpha_2 V_t}\right) - 1\right] - \frac{V+IR_S}{R_{sh}} - I$	$(I_{ph},\ I_{o1}, I_{o2}, R_s, R_{sh},\ \alpha_1,\ \alpha_2)$
SMM	$I = I_{ph} - I_o\left[\exp\left(\frac{V+IR_sN_s}{\alpha N_s V_t}\right) - 1\right] - \frac{V+IR_sN_s}{R_{sh}N_s} - I$	$\left(I_{ph},\ I_o, R_s, R_{sh},\ \alpha\right)$

4. Multi-Approach Gradient-Based Optimizer (MAGBO)

In this study, the GBO algorithm [17] will be improved by adding a new refresh operator and deriving GSR depending on the quasi-Newton method used to solve the optimization problem, while the NRO operator replaces the LEO factor.

4.1. Improve Gradient Search Rule (MGSR)

To minimize the function f then the necessary condition to make x_n is a minimum point of $f(x)$, where $\acute{f}(x) = 0$; in other words, x_n is the solution of the equation $\acute{f}(x) = 0$ and Newton's method is one of the direct methods to find the roots of equation $\acute{f}(x) = 0$, which is at the same time the minimum value of $f(x)$, now, if we use the Taylor series to express the quadratic approximation of $f(x)$ when $x = x_n$, we obtain

$$f(x) = f(x_n) + f'(x_n)(x - x_n) + \frac{f''(x_n)(x - x_n)^2}{2!} \tag{38}$$

Let us make the derivative of Equation (38) equal to zero to obtain the minimum value of $f(x)$

$$f'(x) = f'(x_n) + f''(x_n)(x - x_n) = 0 \tag{39}$$

Now, suppose that x_n is an approximation of the minimum value of $f(x)$, then from Equation (39) we can obtain the special formula for Newton's iterative method,

$$x_{n+1} = x_n - \frac{f'(x_n)}{f''(x_n)} \tag{40}$$

with the necessary condition in more real-world problems, then the function being minimized $f(x)$ is not available in closed form or difficult to differentiable, then the derivatives $f'(x_n)$ and $f''(x_n)$ in Equation (40) can be approximated by a finite difference formula as

$$f''(x_n) = \frac{f(x_n + \Delta x) + f(x_n - \Delta x) - 2f(x_n)}{2\left(\Delta x^2\right)} \tag{41}$$

$$f'(x_n) = \frac{f(x_n + \Delta x) - f(x_n - \Delta x)}{2\Delta x} \tag{42}$$

where Δx is the small step size, so the Equations (41) and (42) are substituted in the equation to obtain

$$x_{n+1} = x_n - \frac{[f(x_n + \Delta x) - f(x_n - \Delta x)]\Delta x}{2[f(x_n + \Delta x) + f(x_n - \Delta x) - 2f(x_n)]} \tag{43}$$

The iterative process indicated by Equation (43) is known as the quasi-Newton method, where $x_n - \Delta x$ represents the previous position and $x_n + \Delta x$ represents the next position.

Then, from Equation (18) we can formulated the proposed $MGSR$ as follows:

$$MGSR = \frac{[f(x_n + \Delta x) - f(x_n - \Delta x)]\Delta x}{2[f(x_n + \Delta x) + f(x_n - \Delta x) - 2x_n]} \tag{44}$$

In view of the ease of dealing with vectors, some modifications are necessary to deal with population-based research, so $x_n - \Delta x$ with x_{best}, $x_n + \Delta x$ is replaced with x_{worst} and (x_n), instead of its fitness $f(x_n)$ are inferred, and the $MGSR$ is reformulated as follows:

$$MGSR = \frac{[y_{an}^m - y_{bn}^m]\Delta x}{2[y_{an}^m + y_{bn}^m - 2x_n]} \tag{45}$$

where Δx is shown in Equation (9), y_{an}^m and y_{bn}^m are computed using Equations (3) and (4), respectively, and x_n is the current solution.

4.2. The Proposed New Refresh Operator (NRO)

Utilizing the idea of Levy flight, the new refresh operator is an approach that was developed to tackle difficult optimization problems as a local search technique. One heuristic approach to solving tough optimization issues is local search. It constantly swaps out the current answer for one of its neighbors to improve upon it. It is known that the search space neighbors of solution x are limitless. As a result, figuring out how to efficiently find a good area is crucial in local searches. It will attempt to generate a new solution at predetermined intervals by merging two random solutions with the best position found up to this point. Developing an efficient strategy for determining the optimal location to conduct the search is essential to this approach. Algorithm 1 displays the new refresh operator (NRO). During the optimization process, it will be utilized within each iteration of the proposed algorithm to enhance the search process.

Algorithm 1: The developed new refresh operator algorithm

Sort the particles in pop^m according to fitness functions
  For *i = 1: Npop*
    Randomly choose two solutions x_{d1}^m and x_{d1}^m from pop^m
    Calculate *the random value z based on* Levyflight for solution *n* by Equation (48)
    Obtain for solution *n* by Equation (47)
    Calculate the new position x_n^{m+1} of solution *n* by Equation (46)
  End For

At first, in each iteration m for a population pop^m with size of N, search agents and a solution $x_n^m = \left(x_{n,1}^m, x_{n,2}^m, \ldots x_{n,dim}^m\right)$ will be generated by GSR as $X1_n^m$ and $X2_n^m$ according to the proposed algorithm and become x_n^{m+1}. After that, this search agent will be enhanced by NRO to become X_n^{m+1} by using this formula:

$$x_n^{m+1} = \begin{cases} x_n^{m+1} + (x_{best} - xp_n^m) + rand \times \left(x_{d1}^m - x_{d2}^m\right) r_1 < 0.5 \\ x_{best} + (x_{best} - xp_n^m) + rand \times \left(x_{d1}^m - x_{d2}^m\right) r_1 > 0.5 \end{cases} \tag{46}$$

where $n = 1, 2, \ldots, \mathrm{N}$, *rand* represent a random number in the range 0 and 1, m denotes to the current iteration, and

$$xp_n^t = x_n^{m+1} + z \times (rand \times (x_{d1}^m - x_{d2}^m))/2 \tag{47}$$

where x_{d1}^m and x_{d1}^m are two solutions chosen randomly from the population pop^m (expect the current particle x_n^m), *rand* is a random number in the range 0 and 1, and t is the number of iterations. In addition, z is random numbers that are generated by the magenta method based on Levy distribution by the following equation:

$$z = 0.01 \times \frac{b \times \omega}{|q|^{\frac{1}{\lambda}}} \tag{48}$$

where b and q are drawn from normal distributions as $b \sim N(0, \lambda^2)$ and $q \sim N(0, \lambda^2)$, λ is constant with value 1.5, and

$$\omega = \sqrt[\lambda]{\frac{\Gamma(1+\lambda) \times \sin\left(\frac{\pi\lambda}{2}\right)}{\Gamma\left[\frac{\lambda+1}{2}\right] \times \lambda \times 2^{\frac{\lambda-1}{2}}}} \tag{49}$$

4.3. Generate New Solutions

Depending on the proposed *MGSR* in Equation (45) and the direction of movement *DM*, we can generate a new position by updating the current position, and its equation can be formulated as follows:

$$X1_n^m = X_n^m - MGSR + DM \tag{50}$$

$$X1_n^m = x_n^m - \frac{[y_{an}^m - y_{bn}^m]\Delta x}{2[y_{an}^m + y_{bn}^m - 2x_n]} + rand \times \rho_2 \times (\, x_{best} - x_n^m \,) \tag{51}$$

$$X2_n^m = x_{best} - MGSR + DM \tag{52}$$

$$X2_n^m = x_{best} - \left[\frac{[y_{an}^m - y_{bn}^m]\Delta x}{2[y_{an}^m + y_{bn}^m - 2x_n]}\right] + rand \times \rho_2 \times (\, x_{r_1} - x_n^m \,) \tag{53}$$

where r_1 are particles chosen randomly from the population pop^m. Accordingly, based on the positions $X1_n^m$, $X2_n^m$, and the current position x_n^m , the new solution at the next iteration will be generated using Equation (17).

By the proposed local search, we can explore its local region and obtain the optimal neighborhood of this particle as described in Algorithm 1.

In the final stage of the proposed local search NRO, the particle x_n^m will be recombined (crossover) with its neighbor x_n^{m+1}, which is obtained by Equation (46) to obtain the best neighbor for the particle x_n^{m+1}.

$$x_n^{m+1} = \begin{cases} x_n^{m+1} & \mu < 0.1 \\ x_n^m & \mu > 0.1 \end{cases} \tag{54}$$

The proposed algorithm pseudo-code is shown in Algorithm 2, and Figure 4 shows the MAGBO essential steps. Figure 5 illustrates the main idea of problem formulation.

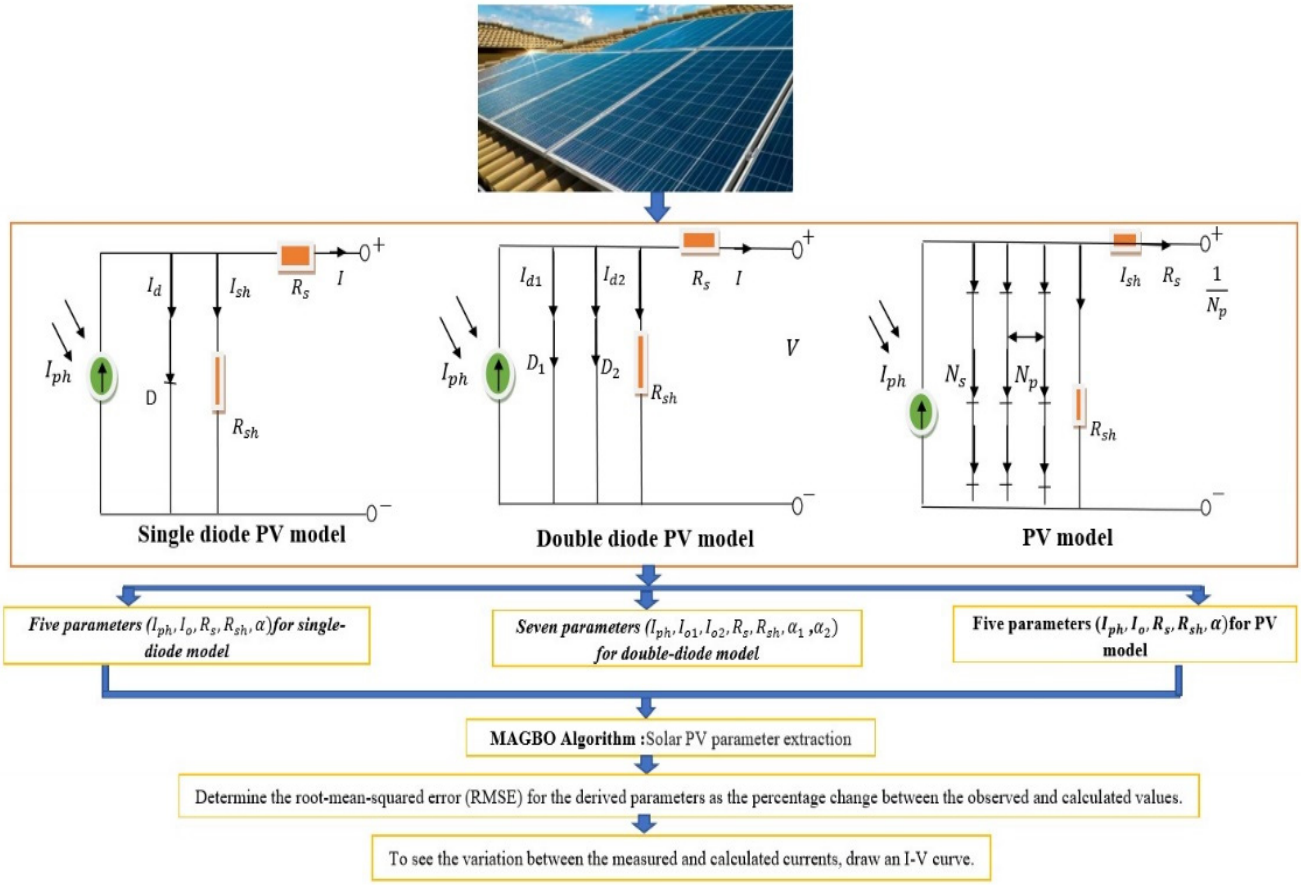

Figure 4. Problem formulation.

Algorithm 2: The MAGBO

Define the set of parameters, *N*, *Tmax*, *dim*, *lb and ub bounds* of feasible region.
Initialize a population of N random solutions.
Calculate *Fitness*, *BestX*, *Best_Cost*, *WorstX*, *Worst_Cost*
While (Termination condition not satisfied) **Do**
  Compute α by Equation (7) and β by Equation (8)
  For $i = 1$: N
    Compute $X1_n^m$ by Equation (51)
    Compute $X2_n^m$ by Equation (53)
      For $j = 1$: *dim*
        Calculate X_n^{m+1} by Equation (17)
        If $rand < 0.5$
          Apply local search technique as Algorithm (1)
        End if
      Apply Crossover operator as equation Equation (54)
    Update *Fitness*, *BestX*, *Best_Cost*, *WorstX*, *Worst_Cost*
  End for
End while

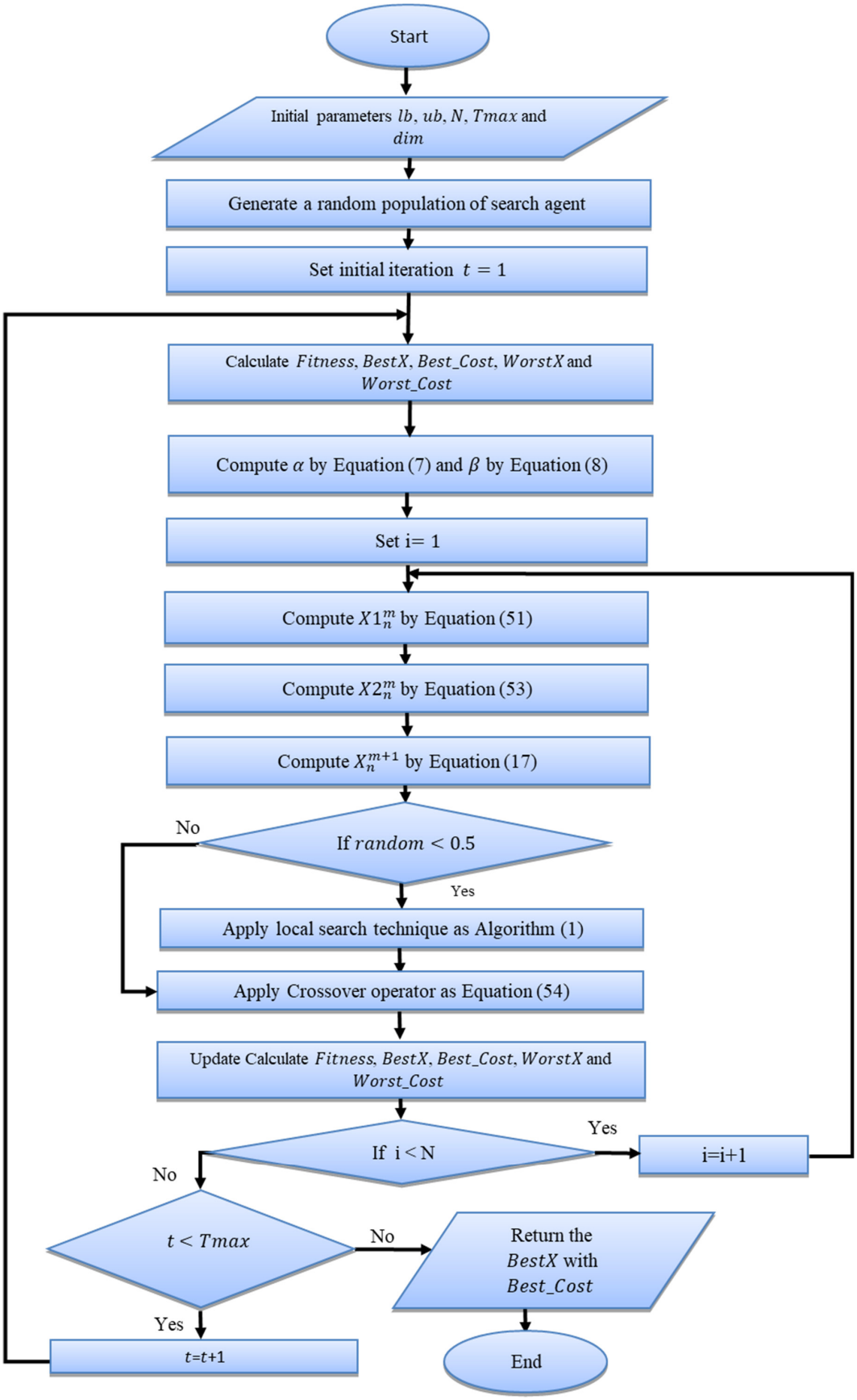

Figure 5. MAGBO Flow chart.

5. Computer Results and Simulations

In this section, the primary objective centers around an in-depth examination of the newly proposed MAGBO algorithm. To ensure a comprehensive analysis, we juxtapose MAGBO against several state-of-the-art algorithms, utilizing the challenging functions from the IEEE CEC 2021 test suite. This rigorous benchmarking offers a solid foundation for assessing MAGBO's optimization capabilities. To supplement the numerical findings, the Wilcoxon signed-rank test, a robust statistical method, is incorporated, lending further weight to the comparative performance claims. Additionally, a qualitative review delves into the intricacies and unique advantages inherent in the MAGBO algorithm. Further fortifying our analysis, MAGBO is applied to the practical task of solar photovoltaic model parameter identification, the results of which are scrutinized through statistical outputs and convergence curve presentations. In the subsequent Section 6, we transition to an introspective reflection on potential challenges and limitations faced during our research, ensuring that the reader is provided a balanced and holistic view of our work, while also hinting at avenues for future improvements.

All of the evaluations for this investigation were carried out on a personal computer operating under the Windows operating system and including a 2.50 GHz Intel Core i5-7300U processor along with 8 gigabytes of random-access memory (RAM). Python was utilized in the implementation of both MAGBO and its rivals.

MAGBO's efficiency was evaluated concerning shifted, rotated, and biased functions using the IEEE CEC 2021 test suite in 20 dimensions. This was done so that MAGBO's performance could be thoroughly investigated by comparing it experimentally to that of rival algorithms. Additional details on the IEEE CEC 2021 test suite may be found in [76].

The experimental data used for the statistical analysis were obtained by carrying out 30 sets of replicated runs, each consisting of 2500 iterations. The MAGBO algorithm will terminate once the maximum number of iterations has been completed. We evaluate the algorithm's performance by comparing the average solution (Avg), the median solution (Med), and the standard deviation. All of this is done without compromising generality (std).

In order to investigate the results of both the MAGBO and the competitors, a pair of non-parametric statistical hypothesis tests called the Friedman test and the Wilcoxon signed-rank test are utilized. The Wilcoxon signed-rank test is used to compare the performance of MAGBO and its competitors across several different metrics, such as how effectively they handle specific tasks, to draw conclusions about which of the two is the superior option. In addition, the Friedman test's final rankings for algorithms on all functions can be used to examine the substantial differences in overall performance between different algorithms.

The effectiveness of the MAGBO is analyzed and compared to that of eight other algorithms throughout the course of this research project. These techniques include GBO [17], EGBO [77], SMA [78], PSO [79], EO [80], SADE [81], CL-PSO [82], and HPSO_TVAC [83]. In this section, we have decided to adhere to the suggestions made by the authors of those other publications concerning the important aspects of competition, and we have outlined them in Table 3.

Table 3. Parameter settings for the competitors.

Algorithm	Parameter Setting
GBO	eps = 0.005 × 10^{-3} × random();
EGBO	LC = 0.7, eps = 5 × 10^{-20} × random()
SMA	z = 0.03
PSO	Vmax = 6, wMax = 0.9, wMin = 0.2, c1 = c2 = 2
EO	V = 1, a1 = 2, a2 = 1, GP = 0.5
SADE	probability = 50, cr = 5m, crm = 0.5, p1 = 0.5

Table 3. *Cont.*

Algorithm	Parameter Setting
JADE	miu_f = 0.5, miu_cr = 0.5, p = 0.1, c = 0.1
CL-PSO	c_local = 1.2, w_min = 0.4, w_max = 0.9, max_flag = 7
HPSO_TVAC	Ci = 0.5, cf = 0.0
MFO	T = $[-1, 1]$, b = 1
LNMHGS	VC2 = 0.03, NP = 50
SSA	c1 = $[2/e, 2]$
MAGBO	eps = $0.005 \times 10^{-3} \times$ random();

5.1. Comparison of MAGBO with State-of-the-Art Competitors Using the IEEE CEC 2021 Test Suite

MAGBO was thoroughly evaluated using the IEEE CEC 2021 test suite, and its results were compared to those of eight other algorithms. The results, shown in Table 4, indicate that MAGBO performed well in terms of average values for most of the test functions, except for f5, f7, and f10. In terms of standard deviation, MAGBO performed significantly better than the other algorithms in almost all cases. These results suggest that MAGBO is a stable, robust, and scalable optimization algorithm that performs well compared to the other algorithms included in the comparison.

The results of the Wilcoxon signed-rank test, which was conducted with a significance level of 0.05, are summarized in Table 5. These results show that MAGBO outperformed several other algorithms, including HPSO_TVAC, CL-PSO, and PSO, in all CEC 2021 test functions. In addition, MAGBO outperformed EGBO, GBO, SMA, and EO on nine functions and SADE on seven functions. These results suggest that MAGBO is a strong performer among the algorithms included in the comparison.

According to Table 4, the convergence rate of the algorithm is improved by using a GBO with a crossover mechanism, the NRO local search technique, and a modified gradient search rule based on the quasi-Newton. Together, the presented methods enable the MAGBO algorithm to generate novel solutions by fusing the properties of two or more existing solutions. This increases the likelihood of finding superior solutions by introducing variety into the solution pool. Keeping the algorithm from settling on a locally optimal solution also facilitates exploration and exploitation. Crossover also makes it easier to probe a wider region of the search space. This is of utmost significance in optimization problems involving complicated and rough landscapes, in which the global optimum may be hidden in a previously undiscovered region. Additionally, the MAGBO algorithm seeks to find a middle ground between exploitation (enhancing the best-known solutions) and exploration (looking for new and perhaps superior answers). While some operators, such as mutation, aid in exploitation, the suggested NRO aids exploration by producing more candidate solutions. In addition, the MAGBO algorithm's convergence can be hastened with the help of a modified gradient search rule based on the quasi-Newton, which may ultimately lead to the generation of superior solutions.

The Wilcoxon signed-rank test showed that MAGBO is a highly reliable optimization technique compared to eight other algorithms. Figure 6 illustrates the convergence behaviors of MAGBO and its competitors on the CEC 2021 test functions. It can be observed that MAGBO significantly outperforms the other algorithms in both initial and final iterations, indicating that it has strong exploration (using swarm intelligence) and exploitation (using quadratic functions) capabilities. In addition, as shown in Figure 6, MAGBO can find the global optimal solution and avoid getting stuck in local optima thanks to its new local search feature. This feature allows the algorithm to explore the solution space more thoroughly and find the best possible solution.

Table 4. Comparison of MAGBO with basics and advanced algorithms.

Algorithm	Criteria	F1	F2	F3	F4	F5	F6	F7	F8	F9	F10	Friedman Avg/Rank	
GBO	Avg	9.217×10^{2}	1.122×10^{3}	1.183×10^{5}	1.907×10^{3}	1.946×10^{4}	2.115×10^{3}	**7.997×10^{3}**	2.332×10^{3}	2.642×10^{3}	3.216×10^{3}	4.44	4.000
	Std	1.415×10^{3}	6.650×10	6.442×10^{5}	0.366×10	1.119×10^{4}	5.474×10^{2}	5.292×10^{3}	0.809×10	1.117×10^{2}	6.647×10		
	Med	4.134×10^{2}	1.101×10^{3}	7.000×10^{2}	1.906×10^{3}	1.944×10^{4}	2.013×10^{3}	7.122×10^{3}	2.334×10^{3}	2.600×10^{3}	3.213×10^{3}		
EGBO	Avg	1.499×10^{2}	1.398×10^{9}	1.183×10^{5}	1.908×10^{3}	**1.280×10^{4}**	3.107×10^{3}	4.270×10^{4}	2.337×10^{3}	2.622×10^{3}	3.208×10^{3}	4.02	3.000
	Std	2.704×10^{2}	7.657×10^{9}	6.442×10^{5}	5.142×10^{0}	1.259×10^{4}	3.569×10^{3}	9.986×10^{4}	0.4241×10	8.419×10	8.238×10		
	Med	1.000×10^{2}	1.100×10^{3}	7.000×10^{2}	1.907×10^{3}	7.881×10^{3}	2.341×10^{3}	8.697×10^{3}	2.336×10^{3}	2.600×10^{3}	3.183×10^{3}		
SMA	Avg	7.679×10^{3}	9.045×10^{5}	9.370×10^{3}	1.904×10^{3}	1.073×10^{5}	2.309×10^{3}	5.924×10^{4}	2.333×10^{3}	2.614×10^{3}	3.160×10^{3}	5.71	6.000
	Std	3.384×10^{3}	7.804×10^{5}	1.662×10^{4}	0.1525×10	4.806×10^{3}	8.531×10^{2}	2.737×10^{4}	0.6499×10	4.880×10	4.418×10		
	Med	8.933×10^{3}	6.705×10^{5}	1.305×10^{3}	1.903×10^{3}	1.053×10^{5}	2.006×10^{3}	5.601×10^{4}	2.300×10^{3}	2.601×10^{3}	3.149×10^{3}		
PSO	Avg	2.137×10^{3}	2.590×10^{5}	2.991×10^{4}	1.905×10^{3}	5.173×10^{4}	1.788×10^{3}	1.203×10^{4}	2.362×10^{3}	2.715×10^{3}	3.278×10^{3}	4.84	5.000
	Std	2.187×10^{3}	3.880×10^{5}	1.418×10^{5}	0.1161×10	2.961×10^{4}	2.248×10^{2}	6.035×10^{3}	5.505×10	3.634×10^{2}	1.597×10^{2}		
	Med	1.453×10^{3}	1.351×10^{5}	7.000×10^{2}	1.903×10^{3}	4.306×10^{4}	1.677×10^{3}	1.063×10^{4}	2.342×10^{3}	2.600×10^{3}	3.232×10^{3}		
EO	Avg	4.280×10^{7}	6.700×10^{9}	1.897×10^{9}	1.907×10^{3}	8.561×10^{4}	6.070×10^{3}	2.166×10^{5}	2.320×10^{3}	3.014×10^{3}	**3.035×10^{3}**	6.52	8.00
	Std	1.346×10^{8}	1.369×10^{10}	2.781×10^{9}	1.179×10	4.972×10^{4}	2.584×10^{3}	6.129×10^{5}	1.135×10	5.436×10^{2}	7.140×10		
	Med	4.233×10^{3}	2.509×10^{6}	5.883×10^{7}	1.903×10^{3}	6.680×10^{4}	5.359×10^{3}	6.654×10^{4}	2.324×10^{3}	2.738×10^{3}	3.017×10^{3}		
SADE	Avg	1.000×10^{2}	1.100×10^{3}	7.000×10^{2}	1.905×10^{3}	5.156×10^{4}	1.672×10^{3}	2.068×10^{4}	2.318×10^{3}	2.615×10^{3}	3.164×10^{3}	3.45	2.000
	Std	0.000	0.000	0.000	7.25×10^{-1}	2.661×10^{4}	1.763×10^{2}	1.239×10^{4}	1.442×10	3.009×10	4.642×10		
	Med	1.000×10^{2}	1.100×10^{3}	7.000×10^{2}	1.905×10^{3}	4.570×10^{4}	1.604×10^{3}	1.719×10^{4}	2.328×10^{3}	2.600×10^{3}	3.158×10^{3}		
CL-PSO	Avg	6.292×10^{6}		1.753×10^{8}	1.913×10^{3}	5.718×10^{4}	2.920×10^{3}	2.040×10^{8}	2.328×10^{3}	2.739×10^{3}	3.423×10^{3}	6.70	9.000
	Std	2.358×10^{7}	5.861×10^{8}	3.641×10^{8}	3.100×10	2.007×10^{4}	1.306×10^{3}	7.703×10^{5}	0.2165×10	3.289×10^{2}	9.664×10^{1}		
	Med	7.389×10^{4}	9.251×10^{5}	7.717×10^{6}	1.906×10^{3}	5.562×10^{4}	2.649×10^{3}	1.648×10^{4}	2.328×10^{3}	2.602×10^{3}	3.443×10^{3}		
HPSO_TVAC	Avg	1.754×10^{4}	1.575×10^{8}	1.554×10^{3}	1.926×10^{3}	5.280×10^{4}	2.163×10^{3}	1.678×10^{4}	2.339×10^{3}	2.647×10^{3}	3.298×10^{3}	6.03	7.000
	Std	6.309×10^{4}	8.617×10^{8}	3.196×10^{3}	1.612×10	2.411×10^{4}	7.765×10^{2}	8.566×10^{3}	0.8417×10	1.382×10^{2}	1.214×10^{2}		
	Med	2.327×10^{3}	1.646×10^{4}	7.000×10^{2}	1.922×10^{3}	4.808×10^{4}	2.000×10^{3}	1.326×10^{4}	2.338×10^{3}	2.600×10^{3}	3.281×10^{3}		
MAGBO	Avg	**1.000×10^{2}**	**1.100×10^{3}**	**7.000×10^{2}**	**1.905×10^{3}**	2.000×10^{4}	**1.659×10^{3}**	8.714×10^{3}	**2.300×10^{3}**	**2.614×10^{3}**	3.237×10^{3}	**2.96**	**1.000**
	Std	0.000	0.000	0.000	0.2648×10	1.103×10^{4}	1.329×10^{2}	5.893×10^{3}	1.059×10	4.880×10	7.765×10		
	Med	1.000×10^{2}	1.100×10^{3}	7.000×10^{2}	1.904×10^{3}	2.080×10^{4}	1.606×10^{3}	7.324×10^{3}	2.329×10^{3}	2.601×10^{3}	3.222×10^{3}		

Table 5. Wilcoxon rank-sum of the MAGBO vs. basic and advanced recent algorithms on CEC2021.

Algorithms	F1	F2	F3	F4	F5	F6	F7	F8	F9	F10
MAGBO vs. GBO	<0.050	<0.050	<0.050	<0.050	0.222171	<0.050	0.680259	<0.050	<0.050	0.266174
MAGBO vs. EGBO	<0.050	<0.050	0.993796	<0.050	<0.050	<0.050	0.379592	<0.050	<0.050	0.070029
MAGBO vs. SMA	<0.050	<0.050	<0.050	0.137504	<0.050	<0.050	<0.050	<0.050	1	<0.05
MAGBO vs. PSO	<0.050	<0.050	0.80952	<0.050	<0.050	<0.050	<0.050	<0.050	<0.050	0.498735
MAGBO vs. EO	<0.050	<0.050	<0.050	0.479204	<0.050	<0.050	<0.050	<0.050	<0.050	<0.050
MAGBO vs. SADE	1	1	1	0.331072	<0.050	<0.050	<0.050	0.063115	<0.050	<0.050
MAGBO vs. CL-PSO	<0.050	<0.050	<0.050	<0.050	<0.050	<0.050	<0.050	0.379592	0.114461	<0.050
MAGBO vs. HPSO_TVAC	<0.050	<0.050	<0.050	<0.050	<0.050	<0.050	<0.050	<0.050	<0.050	<0.050

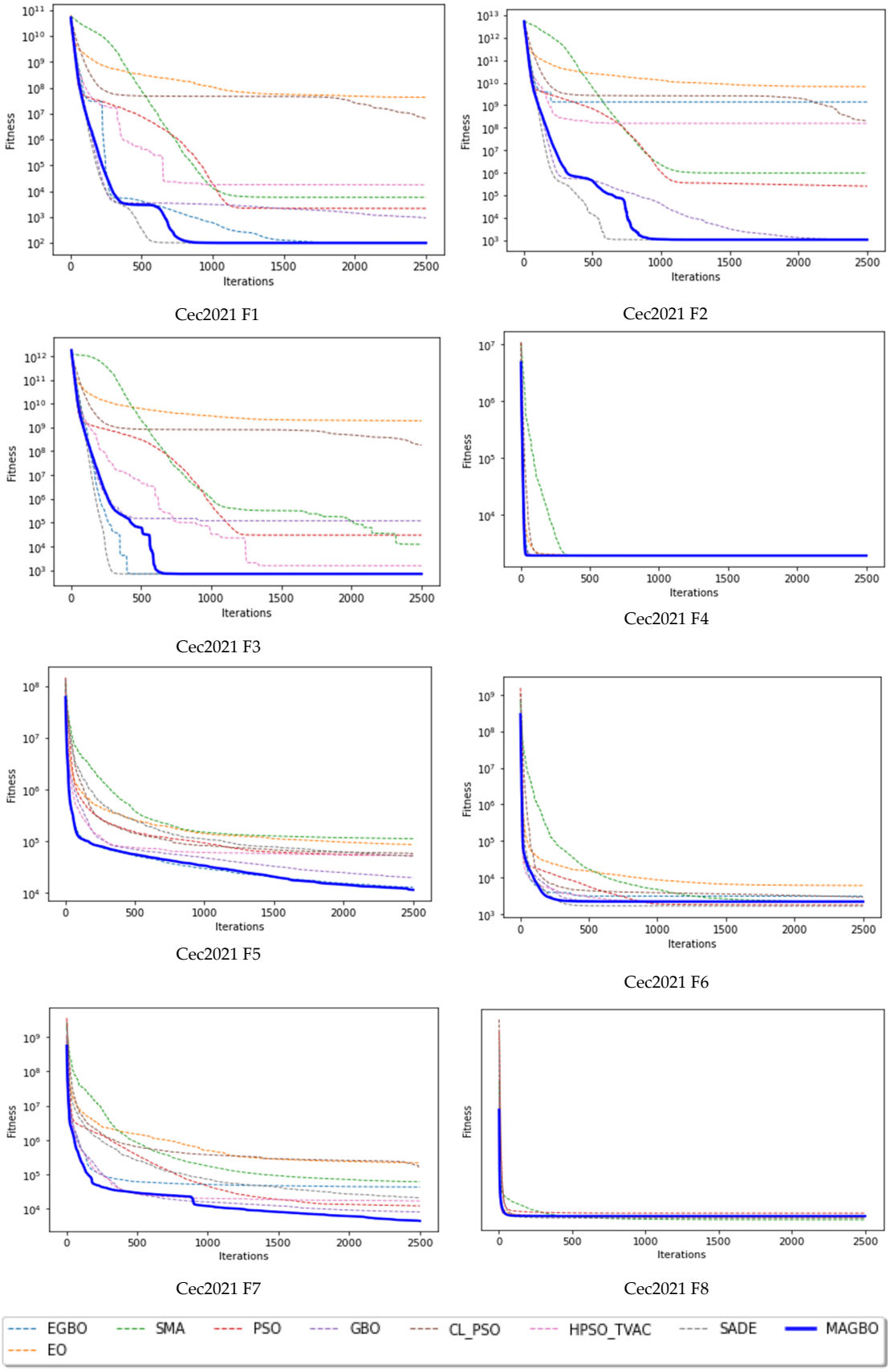

Figure 6. MAGBO convergence curves vs. some basics and advanced algorithms during 2500 iterations.

5.2. Qualitative Analysis of MAGBO

The researchers in this article combined a multi-strategy—the modified gradient search rule (MGSR) derived from the quasi-Newton method to improve its local and global capabilities, a new refresh operator (NRO) to enhance solution quality and algorithm exploration abilities, and a crossover mechanism to balance exploitation and boost the population's variety—to create a novel approach (MAGBO) that overcomes the shortcomings of the standard GBO.

MAGBO is a new method for dealing with GBO-related problems such as uneven exploration and exploitation, premature convergence, and population heterogeneity. Functions 1, 2, 3, 8, and 9 are chosen as exemplary examples from the CEC 2021 set for this study. These procedures were picked because they effectively demonstrate both unimodal and multimodal features.

As part of a qualitative study of the system's performance, Figure 7 gives an in-depth look at how MAGBO acts when looking for solutions in unimodal and multimodal functions. The graph makes it easy to see where MAGBO stands and how fit it is at any given time during the search. This shows the average global fitness level of MAGBO over the exploration and exploitation phases. MAGBO's location in the first dimension is also shown on the graph, along with its evolution through time. The variations in MAGBO's global best fitness (mean) throughout the iterations show how its normal fitness level varies. This visual depiction accurately depicts the research and development stages of MAGBO throughout the entire refinement process.

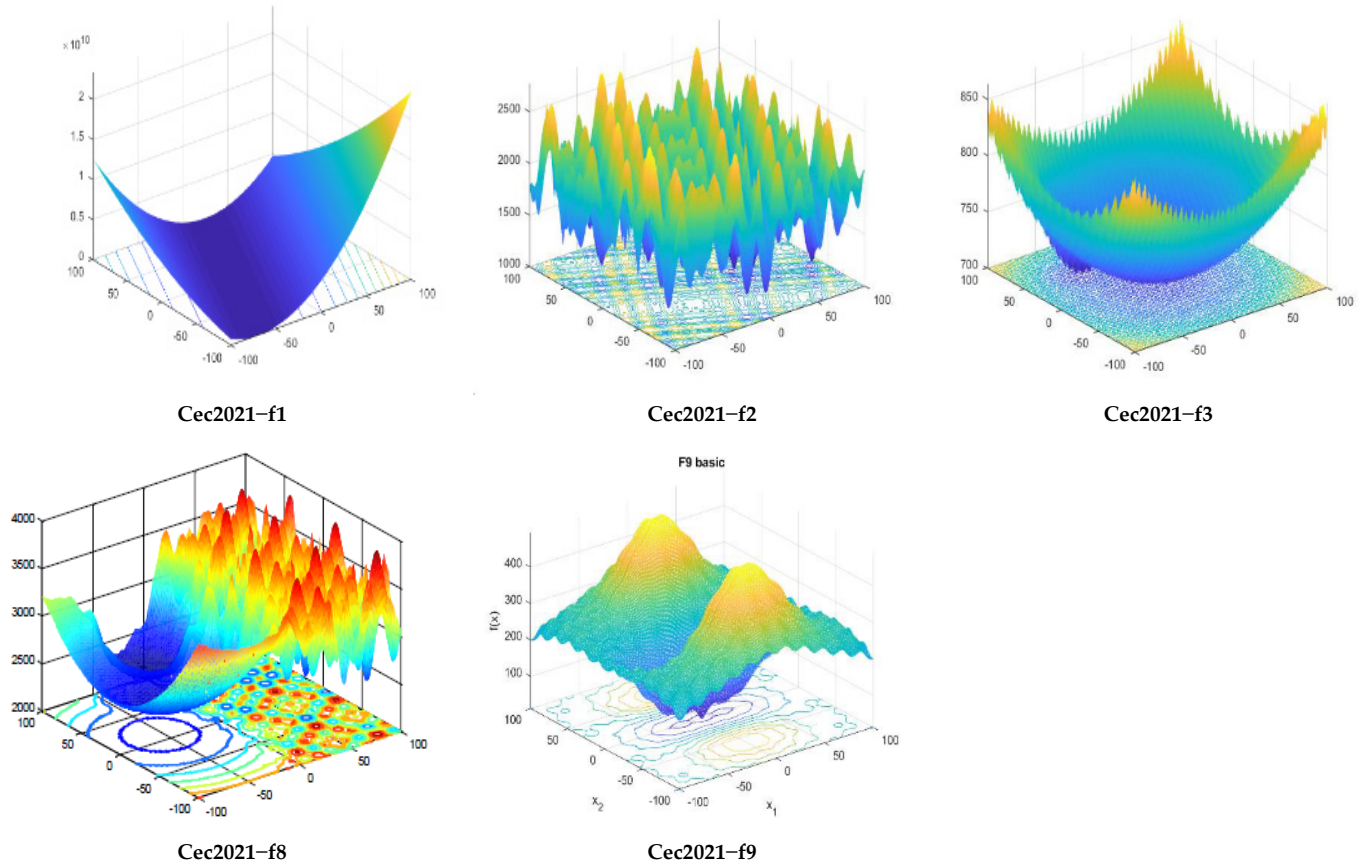

(**a**)

Figure 7. *Cont.*

Cec2021−f1 **Cec2021−f2** **Cec2021−f3**

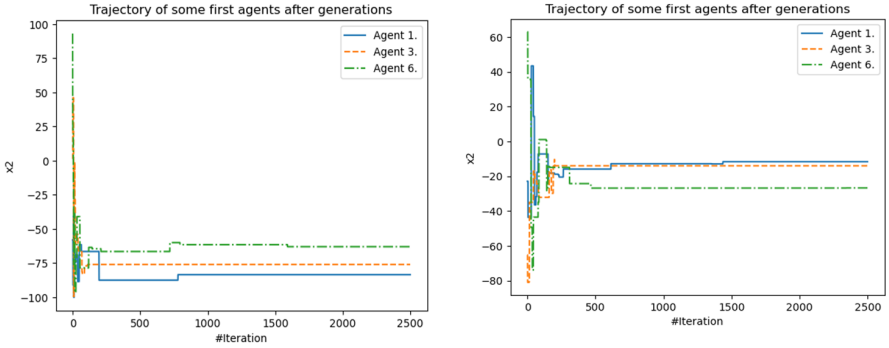

Cec2021−f8 **Cec2021−f9**

(b)

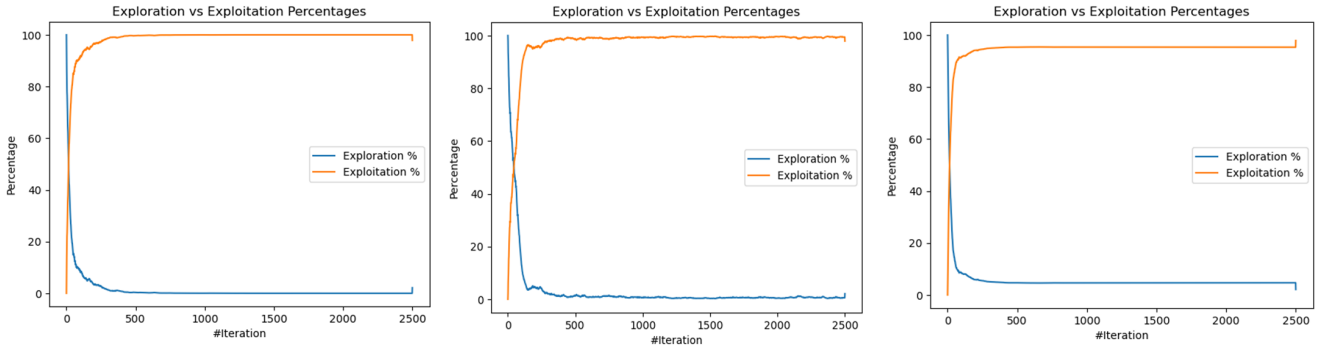

Cec2021−f1 **Cec2021−f2** **Cec2021−f3**

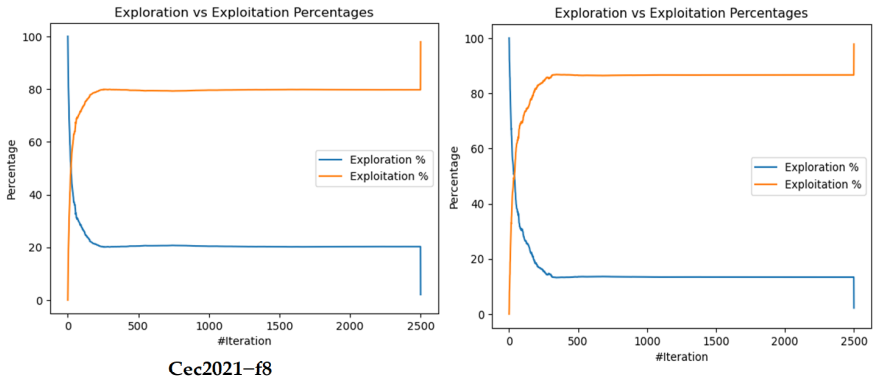

Cec2021−f8 **Cec2021−f9**

(c)

Figure 7. *Cont.*

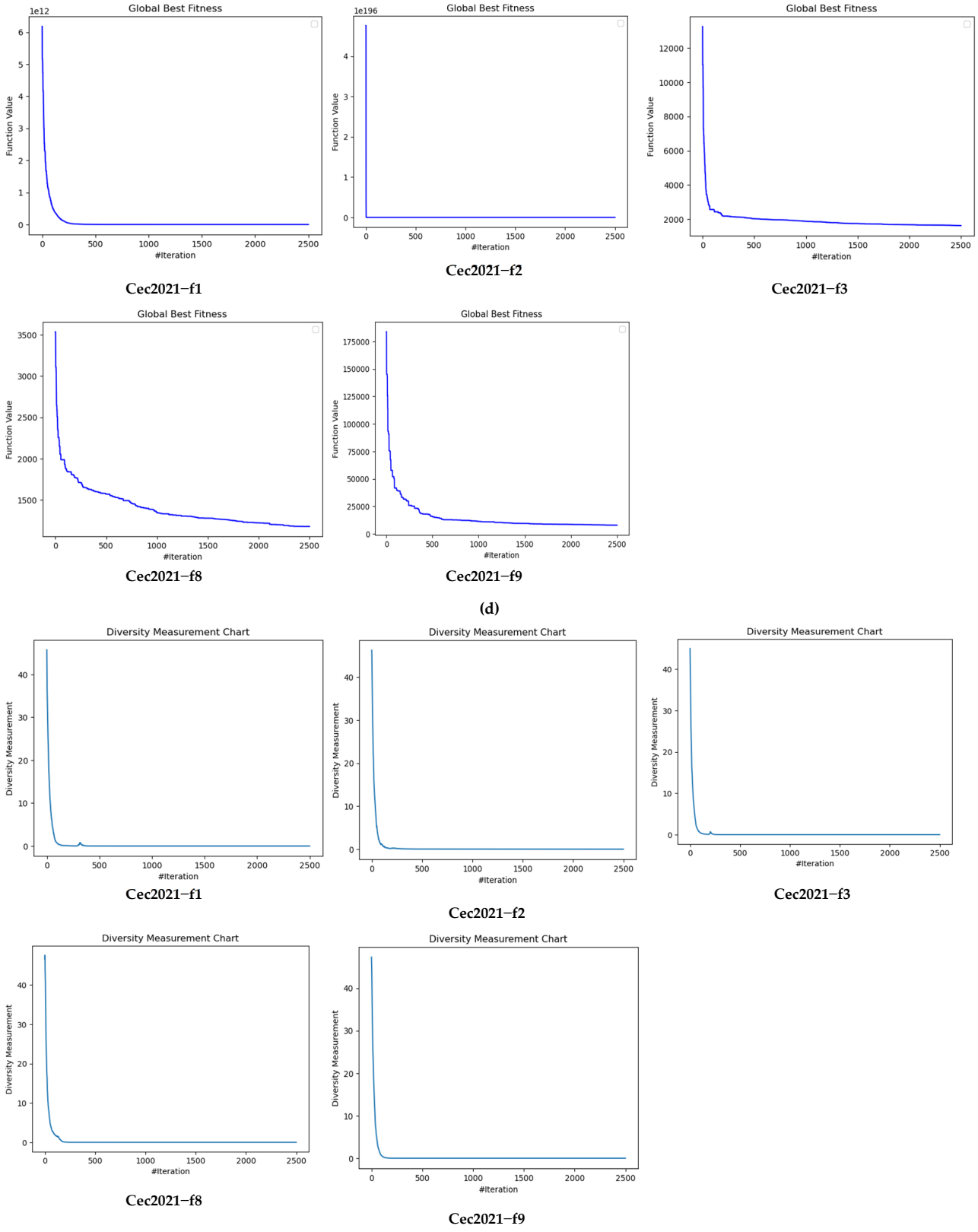

Figure 7. (**a**) MAGBO qualitative analysis (Cec2021_functions). (**b**) MAGBO qualitative analysis (first-dimensional trajectory). (**c**) MAGBO qualitative analysis (phase of exploration and exploitation). (**d**) MAGBO qualitative analysis (global best fitness—average). (**e**) MAGBO qualitative analysis (diversity analysis—average).

MAGBO's primary purpose of exploration is best illustrated by the fact that its first-dimensional trajectory can represent multiple regions of the search space. The MAGBO particle can quickly and correctly find the optimal solution thanks to its rapid oscillation during the prophase and moderate oscillation during the anaphase. Figure 7b shows that MAGBO's location curve has a fairly large amplitude early on, which could cover as much as half of the exploration zone. The position amplitude of a MAGBO particle diminishes with time if the function is smooth. However, the position amplitude also shows substantial changes when the function amplitudes are in flux. This exemplifies the flexibility and dependability of MAGBO in many contexts. Depending on the point of view, the changes in amplitude can seem either spectacular or subtle. MAGBO's substantial early fluctuations attest to the strength of its search skills, while the subtle alterations later on attest to the persistence with which it seeks to locate the ideal solution.

Figure 7c is a graphical representation of MAGBO's discovery and development processes. The graph has two curves, one blue for the exploration phase and one orange for the exploitation phase of the method. Due to a smaller percentage of exploration relative to exploitation, the initial MAGBO displays a larger exploration ratio, as illustrated in Figure 7c. However, as the iteration count rises, the algorithm begins to shift its attention from exploration to exploitation for the vast majority of the chosen functions. This continuous pattern guarantees that MAGBO always keeps the right balance between exploration and exploitation.

Figure 7d, which depicts an average global fitness curve, shows that MAGBO's fitness varies when using the iterative method. The curve has a lot of wiggle room, as can be seen by looking at it closely. The average fitness value drops monotonically with increasing iterations, as does the frequency of oscillation. This indicates that MAGBO searches exhaustively during the anaphase and quickly converges on a solid solution.

The outcomes of diversity analysis on the CEC2021 dataset using the MAGBO algorithm are presented in Figure 7e. The depicted graph illustrates the relationship between the number of iterations and the diversity measure, with the horizontal axis representing the former and the vertical axis representing the latter. The process commences by initializing the population with a random generation, leading to increased levels of diversity during the initial phases. As the iterations go, diversity gradually decreases. It is important to acknowledge that the CEC2021 dataset has a wide range of functions, including unimodal, multimodal, hybrid, and composition functions.

The visual representation presented in Figure 7e clearly demonstrates that MAGBO regularly displays a more pronounced decrease in average diversity across different functions. The aforementioned finding indicates the overall accelerated convergence rate of the MAGBO algorithm. Moreover, the findings highlight the general dominance of MAGBO in terms of its performance, making it a viable option for a diverse range of purposes. The primary cause of this phenomenon can be traced to the integration of a "Crossover mechanism" as outlined in Equation (54) within the MAGBO algorithm.

The inclusion of this mechanism in the MAGBO algorithm grants it the capacity to produce innovative solutions through the amalgamation of attributes derived from two or more parent solutions. As a result, the introduction of variation within the population of solutions serves to prevent early convergence and increases the likelihood of finding superior solutions. Furthermore, the integration of crossover facilitates a thorough investigation of the solution space. This characteristic is of great importance in optimization issues that are characterized by complex and uneven terrains, where the global optimum solution may be located in a distant and unexplored area.

However, it is crucial to emphasize that the effectiveness of crossover depends on the particular problem being addressed and the design of the crossover operator. In specific cases, the use of unsuitable crossover operators or parameter settings can hinder the effectiveness of bio-inspired algorithms. Therefore, it is crucial to carefully design and refine every aspect of the algorithm, such as the crossover mechanism, to correspond with the unique characteristics of the optimization problem being addressed.

5.3. The Suggested Approach for Identification of Solar Photovoltaic Model Parameters

In this study, MAGBO is applied to three different models to show its efficiency: the single, double, and PV models. The benchmark data used in this study from [84] were collected from 36 polycrystalline PV cells and a monocrystalline STM6-40/36 module, both under conditions of 1000 W/m2 irradiation and at different temperatures. These data have been widely used to evaluate different methods for estimating PV model parameters. In previous research, the parameter ranges for PV cells and modules have been kept constant across all studies to ensure a consistent search space. As shown in Table 6, the parameter ranges for PV cells and modules are provided. Eight algorithms were selected for comparison; the population size N is 30, the maximum frequency is 600 (18,000 maximum evaluation), and the number of independent runs is 30.

Table 6. The parameter search ranges.

Parameter	Single/Double Diode		PV Module		STM6-40/36Module	
	Lower	Upper	Lower	Upper	Lower	Upper
$I_{ph}(A)$	0	1	0	2	0	2
$I_{sd}, I_{sd1}, I_{sd2}(\mu A)$	0	1	0	50	0	50
$R_s(\Omega)$	0	0.5	0	2	0	0.36
$R_{sh}(\Omega)$	0	100	0	2000	0	1000
n, n_1, n_2	1	2	1	50	1	60

5.3.1. The Single-Diode Model

The single-diode module's current-voltage (I-V) and voltage-current (P-V) curves are displayed. Figure 8 illustrates the MAGBO mistake that was present on the diode. As shown in Table 7, MAGBO achieved the best results compared to other algorithms; therefore, it is reasonable to conclude that MAGBO possesses the potential to be an effective instrument for the identification of SDM. In addition, Figure 9 illustrates the absolute and relative differences in current value that are shown by making a comparison between the data that were simulated and the data that were observed.

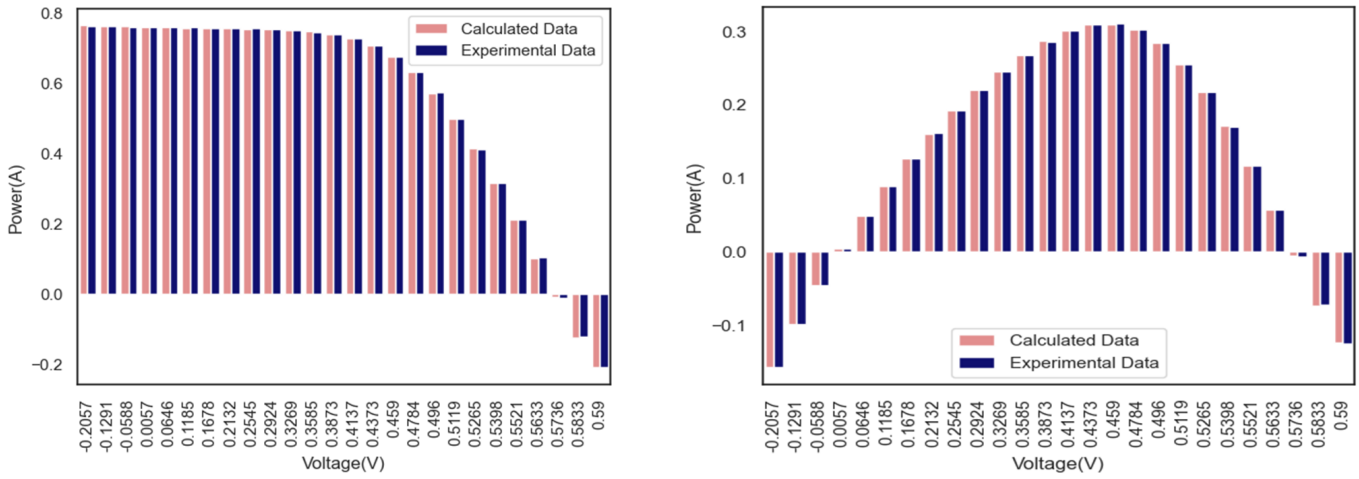

(**a**) (**b**)

Figure 8. Experimental and simulated current-voltage I–V (**a**) and power-voltage (P–V) characteristics (**b**) for a single diode by MAGBO.

The values of five parameters and the RME are presented in Table 8, demonstrating that the suggested method generates superior results compared to other algorithms already in use. The findings above suggest that the proposed method could be utilized as an efficient approach to the localization of single-diode models (SDM).

Table 7. Absolute MAGBO error (IAE) on the single-diode SDM.

Item	Measured Data		Simulated Current Data		Simulated Power Data	
	$V(V)$	$I(A)$	$I_{sim}(A)$	$IAE_I(A)$	$P_{sim}(W)$	$IAE_P(W)$
1	−0.2057	0.7640	0.7640877040	0.0000877040	−0.1571728407	0.0000180407
2	−0.1291	0.7620	0.7626630860	0.0006630860	−0.0984598044	0.0000856044
3	−0.0588	0.7605	0.7613553070	0.0008553070	−0.0447676921	0.0000502921
4	0.0057	0.7605	0.7601539910	0.0003460090	0.0043328777	0.0000019723
5	0.0646	0.7600	0.7590552080	0.0009447920	0.0490349664	0.0000610336
6	0.1185	0.7590	0.7580423450	0.0009576550	0.0898280179	0.0001134821
7	0.1678	0.7570	0.7570916530	0.0000916530	0.1270399794	0.0000153794
8	0.2132	0.7570	0.7561413640	0.0008586360	0.1612093388	0.0001830612
9	0.2545	0.7555	0.7550868720	0.0004131280	0.1921696089	0.0001051411
10	0.2924	0.7540	0.7536638780	0.0003361220	0.2203713179	0.0000982821
11	0.3269	0.7505	0.7513909660	0.0008909660	0.2456297068	0.0002912568
12	0.3585	0.7465	0.7473538510	0.0008538510	0.2679263556	0.0003061056
13	0.3873	0.7385	0.7401172220	0.0016172220	0.2866474001	0.0006263501
14	0.4137	0.7280	0.7273822250	0.0006177750	0.3009180265	0.0002555735
15	0.4373	0.7065	0.7069726520	0.0004726520	0.3091591407	0.0002066907
16	0.4590	0.6755	0.6752801530	0.0002198470	0.3099535902	0.0001009098
17	0.4784	0.6320	0.6307582750	0.0012417250	0.3017547588	0.0005940412
18	0.4960	0.5730	0.5719283620	0.0010716380	0.2836764676	0.0005315324
19	0.5119	0.4990	0.4996070240	0.0006070240	0.2557488356	0.0003107356
20	0.5265	0.4130	0.4136487990	0.0006487990	0.2177860927	0.0003415927
21	0.5398	0.3165	0.3175101190	0.0010101190	0.1713919622	0.0005452622
22	0.5521	0.2120	0.2121549510	0.0001549510	0.1171307484	0.0000855484
23	0.5633	0.1035	0.1022513260	0.0012486740	0.0575981719	0.0007033781
24	0.5736	−0.0100	−0.0087175240	0.0012824760	−0.0050003718	0.0007356282
25	0.5833	−0.1230	−0.1255073910	0.0025073910	−0.0732084612	0.0014625612
26	0.5900	−0.2100	−0.2084723020	0.0015276980	−0.1229986582	0.0009013418

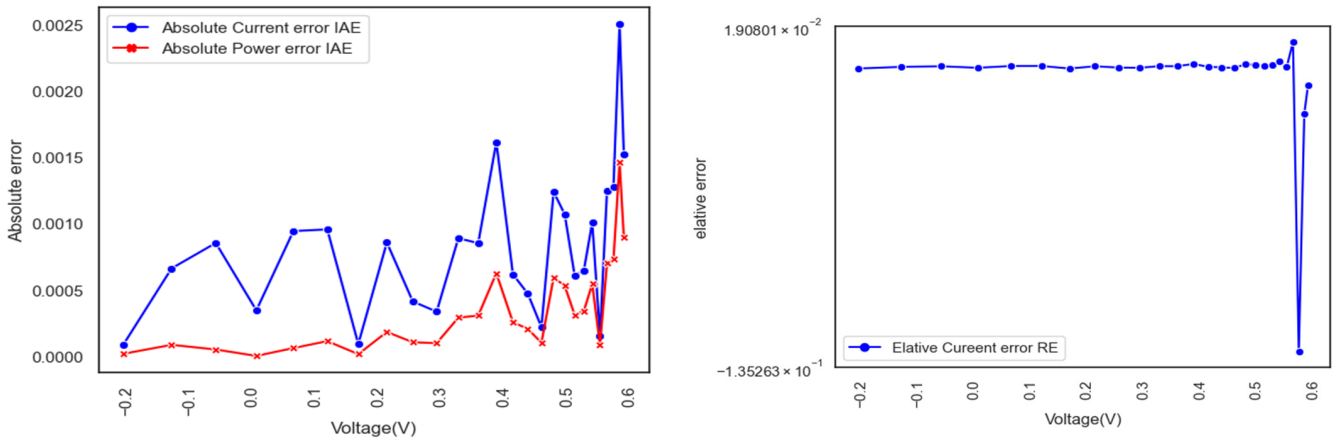

(**a**) (**b**)

Figure 9. Experimental and simulated current data error-index values of SDM: (**a**) IAE; (**b**) RE.

Table 8. A comparison of various algorithms applied to the model of a single-diode SDM.

Algorithm	$I_{ph}(A)$	$I_{sd}(\mu A)$	$R_s(\Omega)$	$R_{sh}(\Omega)$	n	RMSE
MAGBO	$\mathbf{7.60775530\times10^{-7}}$	$\mathbf{3.23020770\times10^{-7}}$	$\mathbf{3.63770933\times10^{-2}}$	$\mathbf{5.37185214\times10}$	$\mathbf{0.148118358\times10}$	$\mathbf{9.860218779287832\times10^{-4}}$
PSO	$7.60830725 \times 10^{-1}$	$2.97833118 \times 10^{-7}$	$3.67049082 \times 10^{-2}$	5.15209651×10	0.147305453×10	$9.981852770215333 \times 10^{-4}$
PGJAYA	$7.60777374 \times 10^{-1}$	$3.22628317 \times 10^{-7}$	$3.63818340 \times 10^{-2}$	5.36737322×10	0.148106137×10	$9.860248538038482 \times 10^{-4}$
IJAYA	$7.60656504 \times 10^{-1}$	$3.29562058 \times 10^{-7}$	$3.62293998 \times 10^{-2}$	5.37054978×10	0.148323279×10	$9.963586798743776 \times 10^{-4}$
MLBSA	$7.60774976 \times 10^{-1}$	$3.23425701 \times 10^{-7}$	$3.63719322 \times 10^{-2}$	5.37466051×10	0.148130985×10	$9.860248926943814 \times 10^{-4}$
CL-PSO	$7.60360878 \times 10^{-1}$	$5.44600932 \times 10^{-7}$	$3.48181218 \times 10^{-2}$	9.60050380×10	0.153544041×10	$1.6631313822752311 \times 10^{-3}$
HPSO_TVA	$7.60711254 \times 10^{-1}$	$3.48500520 \times 10^{-7}$	$3.60688873 \times 10^{-2}$	5.60201199×10	0.148886781×10	$9.967934554405249 \times 10^{-4}$
PSO_W	$7.60768649 \times 10^{-1}$	$3.24287287 \times 10^{-7}$	$3.63625558 \times 10^{-2}$	5.38923057×10	0.148157655×10	$9.860565785062050 \times 10^{-4}$
GBO	$7.60776465 \times 10^{-1}$	$3.22245709 \times 10^{-7}$	$3.63871340 \times 10^{-2}$	5.36607682×10	0.148094154×10	$9.860328319688564 \times 10^{-4}$

5.3.2. Double-Diode Module Results (DDM)

Figure 10 compares the actual observed data and the estimated model properties that MAGBO provided. Figure 11 presents a graphical representation of a double-diode module's RE and IAE values. The simulated current-voltage (I-V) and power-voltage (P-V) characteristic curves are an excellent match for the experimental data collected. The simulation results are presented in Table 9, which includes the current, power, IAE, and RE numbers. The results presented in Table 9 demonstrate that MAGBO's double-diode module successfully reproduces the primary properties of solar cells. Table 10 presents the results of comparisons between the performance of MAGBO and that of alternative algorithms. Table 10 presents the RMSE comparison findings and the values of the seven extracted parameters taken out of the model. Compared to the other seven methods, the Root Mean Square Error (RMSE) for the suggested MAGBO is as low as possible. Table 10 presents the results of comparisons between the performance of MAGBO and that of alternative algorithms. Table 10 presents the RMSE comparison findings and the values of the seven extracted parameters taken out of the model. When contrasted with the other seven approaches, the RMSE for the proposed MAGBO is the lowest it can be.

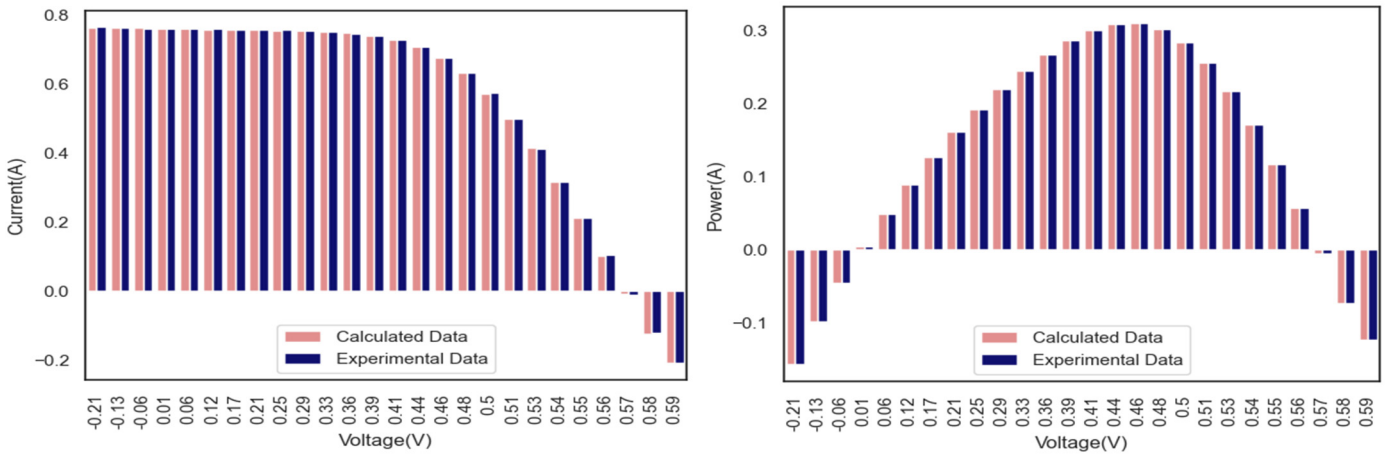

(**a**) (**b**)

Figure 10. Experimental and simulated current-voltage I–V (**a**) and power-voltage (P–V) characteristics (**b**) for a double diode by MAGBO.

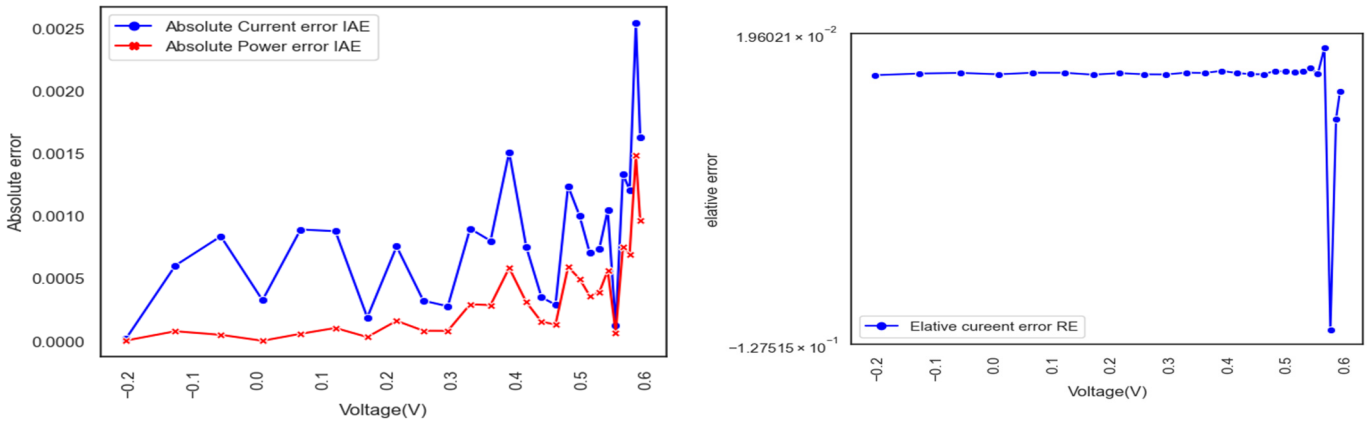

(**a**) (**b**)

Figure 11. Experimental and simulated current data error-index values of SDM: (**a**) IAE; (**b**) RE.

Table 9. Absolute MAGBO error (IAE) on the double-diode DDM.

Item	Measured Data		Simulated Current Data		Simulated Power Data	
	$V(V)$	$I(A)$	$I_{sim}(A)$	$IAE_I(A)$	$P_{sim}(W)$	$IAE_P(W)$
1	−0.2057	0.7640	0.7639834360	0.0000165640	−0.1571513928	0.0000034072
2	−0.1291	0.7620	0.7626041160	0.0006041160	−0.0984521914	0.0000779914
3	−0.0588	0.7605	0.7613377140	0.0008377140	−0.0447666576	0.0000492576
4	0.0057	0.7605	0.7601738000	0.0003262000	0.0043329907	0.0000018593
5	0.0646	0.7600	0.7591076900	0.0008923100	0.0490383568	0.0000576432
6	0.1185	0.7590	0.7581214260	0.0008785740	0.0898373890	0.0001041110
7	0.1678	0.7570	0.7571886170	0.0001886170	0.1270562499	0.0000316499
8	0.2132	0.7570	0.7562436060	0.0007563940	0.1612311368	0.0001612632
9	0.2545	0.7555	0.7551772970	0.0003227030	0.1921926221	0.0000821279
10	0.2924	0.7540	0.7537223450	0.0002776550	0.2203884137	0.0000811863
11	0.3269	0.7505	0.7513991210	0.0008991210	0.2456323727	0.0002939227
12	0.3585	0.7465	0.7473014250	0.0008014250	0.2679075609	0.0002873109
13	0.3873	0.7385	0.7400106390	0.0015106390	0.2866061205	0.0005850705
14	0.4137	0.7280	0.7272469310	0.0007530690	0.3008620554	0.0003115446
15	0.4373	0.7065	0.7068502790	0.0003502790	0.3091056270	0.0001531770
16	0.4590	0.6755	0.6752105300	0.0002894700	0.3099216333	0.0001328667
17	0.4784	0.6320	0.6307607540	0.0012392460	0.3017559447	0.0005928553
18	0.4960	0.5730	0.5719947380	0.0010052620	0.2837093900	0.0004986100
19	0.5119	0.4990	0.4997061470	0.0007061470	0.2557995766	0.0003614766
20	0.5265	0.4130	0.4137336890	0.0007336890	0.2178307873	0.0003862873
21	0.5398	0.3165	0.3175462240	0.0010462240	0.1714114517	0.0005647517
22	0.5521	0.2120	0.2121230160	0.0001230160	0.1171131171	0.0000679171
23	0.5633	0.1035	0.1021632990	0.0013367010	0.0575485863	0.0007529637
24	0.5736	−0.0100	−0.0087917210	0.0012082790	−0.0050429312	0.0006930688
25	0.5833	−0.1230	−0.1255433950	0.0025433950	−0.0732294623	0.0014835623
26	0.5900	−0.2100	−0.2083715350	0.0016284650	−0.1229392057	0.0009607943

5.3.3. PV Module (PV)

Figure 12 illustrates the high degree of consistency between the simulated and collected data, with I-V and P-V curves that are realistic approximations of the properties of the Photowatt-PWP 201 module model. Figure 13 displays the experimentally gathered and computer-generated representations of observed currents for the IAE and RE of the PV module model. Table 11 presents the findings of this experiment, including the current, power, IAR, and RE values, which support the idea that the values proposed by MAGBO for the model parameters of the PV modules are reliable. Table 12 lists the best RMSE score and the five extracted parameter values from each of the seven techniques' total of 30 tests. In conclusion, the proposed MAGBO performs better than other methods in forecasting the parameters of PV module models compared to other methods.

5.3.4. Statistical Results and Convergence Curves

Table 13 provides a summary of the statistical information on competing algorithms. (after carrying out 30 separate runs, each of which consisted of 600 iterations) The statistical data are presented in Table 13 as best, worst, Avg, std, and Rank values. By examining these numbers, we can deduce that MAGBO achieves the best results within 30 independent trials with a Rank (Friedman test) of 1. On a single-diode module, a double-diode module, and a PV module, MAGBO performs at a generally competitive level with the most recent robust algorithm. Figure 14 displays the convergence curves of the MAGBO method and those of its competitors.

Table 10. A comparison of various algorithms applied to the model of a double-diode DDM.

Algorithm	$I_{ph}(A)$	$I_{sd1}(\mu A)$	$I_{sd2}(\mu A)$	$R_s(\Omega)$	$R_{sh}(\Omega)$	n_1	n_2	RMSE
MAGBO	$\mathbf{7.60781094 \times 10^{-1}}$	$\mathbf{2.25969455 \times 10^{-7}}$	$\mathbf{3.67404535 \times 10^{-2}}$	$\mathbf{5.54852834 \times 10}$	$\mathbf{0.145101498 \times 10}$	$\mathbf{7.49386194 \times 10^{-7}}$	$\mathbf{0.200000000 \times 10}$	$\mathbf{9.82484851996943 \times 10^{-4}}$
PSO	$7.60818668 \times 10^{-1}$	$1.92236886 \times 10^{-7}$	$3.70214586 \times 10^{-2}$	5.49831144×10	0.143704875×10	$9.69884458 \times 10^{-7}$	0.199958878×10	$9.860071193600016 \times 10^{-4}$
PGJAYA	$7.60751928 \times 10^{-1}$	$2.91525289 \times 10^{-7}$	$3.65535114 \times 10^{-2}$	5.51135412×10	0.176996546×10	$2.27698207 \times 10^{-7}$	0.145498866×10	$9.852611722895091 \times 10^{-4}$
IJAYA	$7.60787349 \times 10^{-1}$	$1.66868484 \times 10^{-7}$	$3.65910355 \times 10^{-2}$	5.36663167×10	0.170854351×10	$2.41944586 \times 10^{-7}$	0.145998738×10	$9.860914205884810 \times 10^{-4}$
MLBSA	$7.60780345 \times 10^{-1}$	$2.86499791 \times 10^{-7}$	$3.64993221 \times 10^{-2}$	5.42564433×10	0.147096561×10	$2.63125416 \times 10^{-7}$	0.199999784×10	$9.840561693493248 \times 10^{-4}$
CL-PSO	$7.62937590 \times 10^{-1}$	$1.80424338 \times 10^{-7}$	$3.55917202 \times 10^{-2}$	4.77950471×10	0.144959311×10	$4.20720089 \times 10^{-7}$	0.167893978×10	$1.6430906963831881 \times 10^{-4}$
HPSO_TVA	$7.60769273 \times 10^{-1}$	$3.83641383 \times 10^{-7}$	$3.56754579 \times 10^{-2}$	5.80624538×10	0.149871283×10	0.00000000	0.178885865×10	$1.0402286091084594 \times 10^{-4}$
PSO_W	$7.60770205 \times 10^{-1}$	$3.23613029 \times 10^{-7}$	$3.63706958 \times 10^{-2}$	5.38189735×10	0.148136716×10	$3.29665828 \times 10^{-12}$	0.186219871×10	$9.860319283422937 \times 10^{-4}$
GBO	$7.60777595 \times 10^{-1}$	$3.23396195 \times 10^{-7}$	$3.63727942 \times 10^{-2}$	5.37457057×10	0.148129998×10	$1.33799831 \times 10^{-12}$	0.190873826×10	$9.860264229026566 \times 10^{-4}$

Table 11. Absolute MAGBO error (IAE) on the PV module model.

Item	Measured Data		Simulated Current Data		Simulated Power Data	
	$V(V)$	$I(A)$	$I_{sim}(A)$	$IAE_I(A)$	$P_{sim}(W)$	$IAE_P(W)$
1	0.12480	1.03150	1.0291191620	0.0023808380	0.1284340714	0.0023808380
2	1.80930	1.03000	1.0273810740	0.0026189260	1.8588405772	0.0026189260
3	3.35110	1.02600	1.0257417980	0.0002582020	3.4373633393	0.0002582020
4	4.76220	1.02200	1.0241071560	0.0021071560	4.8770030983	0.0021071560
5	6.05380	1.01800	1.0222918060	0.0042918060	6.1887501352	0.0042918060
6	7.23640	1.01550	1.0199306820	0.0044306820	7.3806263872	0.0044306820
7	8.31890	1.01400	1.0163631070	0.0023631070	8.4550230508	0.0023631070
8	9.30970	1.01000	1.0104961520	0.0004961520	9.4074160263	0.0004961520
9	10.21630	1.00350	1.0006289710	0.0028710290	10.2227257564	0.0028710290
10	11.04490	0.98800	0.9845483790	0.0034516210	10.8742383912	0.0034516210
11	11.80180	0.96300	0.9595216770	0.0034783230	11.3240829276	0.0034783230
12	12.49290	0.92550	0.9228388180	0.0026611820	11.5289330694	0.0026611820
13	13.12310	0.87250	0.8725996630	0.0000996630	11.4512126375	0.0000996630
14	13.69830	0.80750	0.8072742630	0.0002257370	11.0582850369	0.0002257370
15	14.22210	0.72650	0.7283364770	0.0018364770	10.3584742095	0.0018364770
16	14.69950	0.63450	0.6371379980	0.0026379980	9.3656100016	0.0026379980
17	15.13460	0.53450	0.5362130600	0.0017130600	8.1153701779	0.0017130600
18	15.53110	0.42750	0.4295113210	0.0020113210	6.6707832776	0.0020113210
19	15.89290	0.31850	0.3187744780	0.0002744780	5.0662509014	0.0002744780
20	16.22290	0.20850	0.2073895000	0.0011105000	3.3644591196	0.0011105000
21	16.52410	0.10100	0.0961671640	0.0048328360	1.5890758347	0.0048328360
22	16.79870	−0.00800	−0.0083253950	0.0003253950	−0.1398558130	0.0003253950
23	17.04990	−0.11100	−0.1109364920	0.0000635080	−1.8914560950	0.0000635080
24	17.27930	−0.20900	−0.2092472760	0.0002472760	−3.6156464562	0.0002472760
25	17.48850	−0.30300	−0.3008635980	0.0021364020	−5.2616530336	0.0021364020

Table 12. A comparison of various algorithms applied to a single-diode DDM model.

Algorithm	$I_{ph}(A)$	$I_{sd}(\mu A)$	$R_s(\Omega)$	$R_{sh}(\Omega)$	n	RMSE
MAGBO	**1.03051430 × 10**	**3.48226289 × 10^{-6}**	**0.120127101×10**	**9.81982284×10^{2}**	**4.86428348×10**	**2.425074868100019×10^{-3}**
PSO	0.143559362 × 10	0.00000000	0.00000000	1.46242721 × 10	0.100000000 × 10	2.742507777740578100 × 10^{-1}
PGJAYA	0.103079770 × 10	3.30962024 × 10^{-6}	0.120648712 × 10	9.30403403 × 10^{2}	4.84489889 × 10	2.4291524524006703 × 10^{-3}
IJAYA	0.103041596 × 10	3.50647703 × 10^{-6}	0.120112652 × 10	1.00002657 × 10^{3}	4.86687509 × 10	2.4256537082842510 × 10^{-3}
MLBSA	0.103051756 × 10	3.48211561 × 10^{-6}	0.120128062 × 10	9.81736099 × 10^{2}	4.86426751 × 10	2.4250751724230210 × 10^{-3}
CL-PSO	0.102600504 × 10	4.74880673 × 10^{-6}	0.124732241 × 10	7.81089319 × 10^{2}	4.99392076 × 10	1.49624138566545101 × 10^{-2}
HPSO_TVA	0.105173347 × 10	5.05107355 × 10^{-8}	0.153633461 × 10	2.05631823 × 10^{2}	3.64672902 × 10	1.11282483130807390 × 10^{-2}
PSO_W	0.103032474 × 10	3.54993442 × 10^{-6}	0.119961187 × 10	1.01326705 × 10^{2}	4.87162092 × 10	2.4258587696614703 × 10^{-3}
GBO	0.103066014 × 10	3.42682201 × 10^{-6}	0.120289483 × 10	9.60567724 × 10^{2}	4.85816052 × 10	2.4255399509107550 × 10^{-3}

Table 13. MAGBO and other competitors for various PV models.

PV Module	Algorithm	RMSE				Significant Wilcoxon Test Friedman Test/Rank		
		Min	Max	Avg.	Std			
Single-diode model of RTC France	MAGBO	**9.8602×10^{-4}**	**9.8602×10^{-4}**	**9.86022×10^{-4}**	**8.41862×10^{-17}**		**1.206897**	**1**
	PSO	9.94813 × 10^{-4}	3.8151316 × 10^{-2}	2.34396 × 10^{-2}	5.40938 × 10^{-2}	+	8.103448	8
	PGJAYA	9.86025 × 10^{-4}	1.033627 × 10^{-3}	9.94721 × 10^{-4}	1.26863 × 10^{-5}	+	3.482759	3
	IJAYA	9.96359 × 10^{-4}	1.482295 × 10^{-3}	1.13907 × 10^{-3}	1.48842 × 10^{-4}	+	5.586207	6
	MLBSA	9.86022 × 10^{-4}	1.00735 × 10^{-3}	9.88786 × 10^{-4}	4.85071 × 10^{-6}	+	2.241379	2
	CL-PSO	1.663131 × 10^{-3}	3.606517 × 10^{-3}	2.46597 × 10^{-3}	5.03603 × 10^{-4}	+	8.448276	9
	HPSO_TVA	9.96793 × 10^{-4}	2.170638 × 10^{-3}	1.49135 × 10^{-3}	3.40663 × 10^{-4}	+	6.448276	7
	PSO_W	9.86057 × 10^{-4}	3.8151316 × 10^{-2}	2.47509 × 10^{-3}	6.74863 × 10^{-3}	+	5.517241	5
	GBO	9.86033 × 10^{-4}	3.015336 × 10^{-3}	1.11602 × 10^{-3}	4.22836 × 10^{-4}	+	3.965517	4
Double-diode model of RTC France	MAGBO	**9.8248×10^{-4}**	**9.9667×10^{-4}**	**9.84729×10^{-4}**	**2.94950×10^{-6}**		**1.655172**	**1**
	PSO	9.86007 × 10^{-4}	3.8151316 × 10^{-2}	1.23483 × 10^{-2}	1.56943 × 10^{-2}	+	8.241379	9
	PGJAYA	9.85261 × 10^{-4}	1.368534 × 10^{-3}	1.03260 × 10^{-3}	8.03099 × 10^{-5}	+	3.551724	4
	IJAYA	9.86451 × 10^{-4}	1.492106 × 10^{-3}	1.18338 × 10^{-3}	1.73319 × 10^{-4}	+	5	5
	MLBSA	9.84056 × 10^{-4}	1.130151 × 10^{-3}	1.00554 × 10^{-3}	4.14601 × 10^{-5}	+	2.827586	2
	CL-PSO	1.643091 × 10^{-3}	4.408675 × 10^{-3}	2.61184 × 10^{-3}	7.56568 × 10^{-4}	+	8.137931	8
	HPSO_TVA	1.040229 × 10^{-3}	2.686124 × 10^{-3}	1.76918 × 10^{-3}	4.45671 × 10^{-4}	+	7.103448	7
	PSO_W	9.86032 × 10^{-4}	0.03339187	2.38006 × 10^{-3}	5.86805 × 10^{-3}	+	5.482759	6
	GBO	9.82733 × 10^{-4}	2.073028 × 10^{-3}	1.06864 × 10^{-3}	2.28955 × 10^{-4}	+	3	3

Table 13. *Cont.*

PV Module	Algorithm	RMSE				Significant	Wilcoxon Test Friedman Test/Rank	
		Min	Max	Avg.	Std			
PV module model of Photo Watt-PWP 201	MAGBO	$\mathbf{2.42507 \times 10^{-3}}$	$\mathbf{2.42507 \times 10^{-3}}$	$\mathbf{2.42507 \times 10^{-3}}$	$\mathbf{6.15834 \times 10^{-16}}$		1	1
	PSO	$2.74250778 \times 10^{-1}$	$7.83911954 \times 10^{-1}$	3.19336×10^{-1}	9.37310×10^{-2}	+	8.017241	9
	PGJAYA	2.42507×10^{-3}	3.17454×10^{-3}	2.46388×10^{-3}	1.37087×10^{-4}	+	2.965517	3
	IJAYA	2.425654×10^{-3}	2.662246×10^{-3}	2.46927×10^{-3}	5.20336×10^{-5}	+	3.758620	4
	MLBSA	2.42507×10^{-3}	$2.74250778 \times 10^{-1}$	2.06983×10^{-2}	6.89281×10^{-2}	+	2.655172	2
	CL-PSO	1.4962413×10^{-2}	311203745×10^{-1}	1.18115×10^{-1}	8.93019×10^{-2}	+	5.482758	5
	HPSO_TVA	1.1128248×10^{-2}	$2.74250778 \times 10^{-1}$	2.32335×10^{-1}	9.53834×10^{-2}	+	6.793103	6
	PSO_W	2.425859×10^{-3}	$4.42058515 \times 10^{-1}$	2.86844×10^{-1}	9.92052×10^{-2}	+	7.482758	8
	GBO	2.42554×10^{-3}	$2.74250778 \times 10^{-1}$	2.47187×10^{-1}	8.2581072×10^{-2}	+	6.844827	7

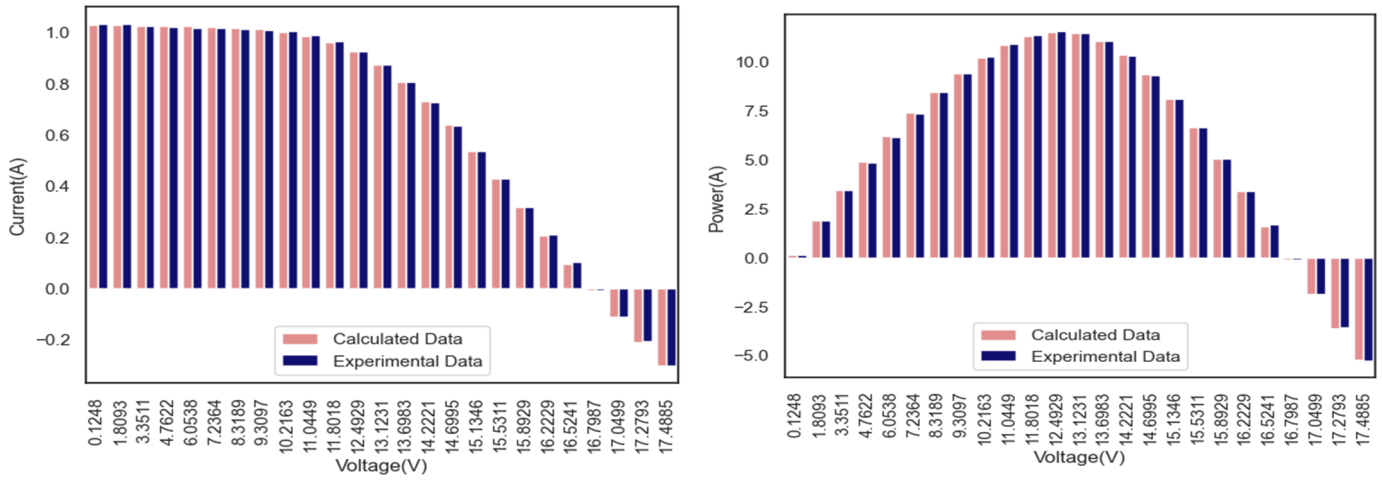

(**a**) (**b**)

Figure 12. Experimental and simulated current-voltage I-V (**a**) and power-voltage (P-V) characteristics (**b**) for a PV module model by MAGBO.

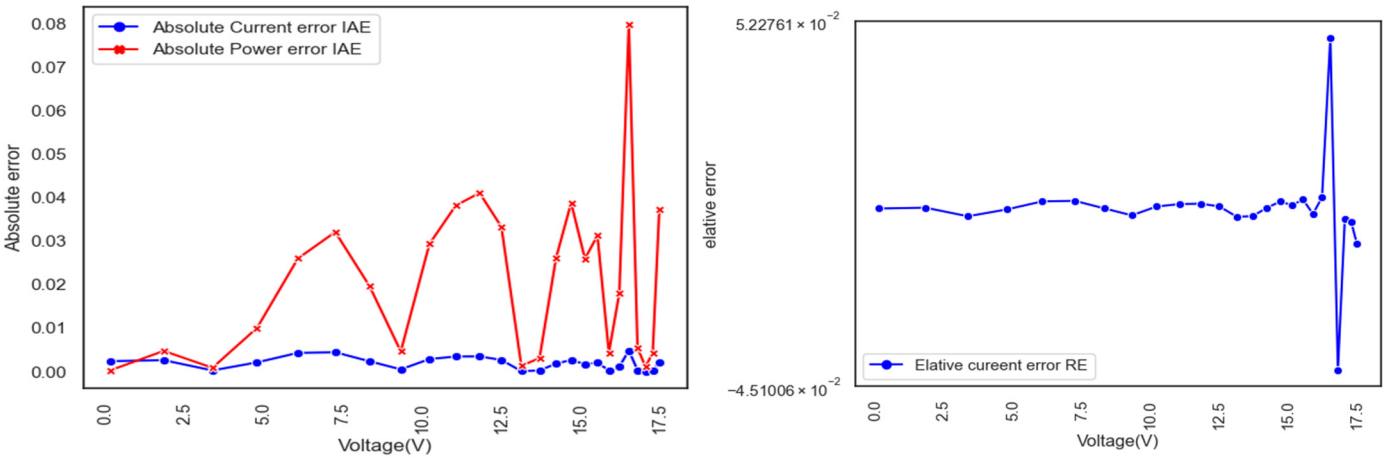

(**a**) (**b**)

Figure 13. Experimental and simulated current data error-index values of a PV module model: (**a**) IAE; (**b**) RE.

5.4. Tests MAGBO on a Wide Selection of Solar Cells and Modules

Data from the PVM 752 GaAs thin-film cell at 25 °C and total irradiation (1000 W/m^2) and the STP6-40/36 module are used to prove the validity and reliability of MAGBO, a method for detecting the properties of both the SDM and DDM of photovoltaic modules. The simulation parameters were determined using 44 pairs of I-V points from the PVM 752 cell [85] and data from the STP6-40/36 module, which consisted of 36 series-connected polycrystalline cells and were tested at temperatures of 51 °C and 55 °C, along with measurements at varying temperatures and irradiance levels. Table 6 details how we used actual data from STM6-40/36 and PVM 752 GaAs thin-film modules to determine the simulation experiment's settings. The parameters of the compared algorithms are listed in Table 3. Each issue runs using the same maximum number of iterations (600) across all methods.

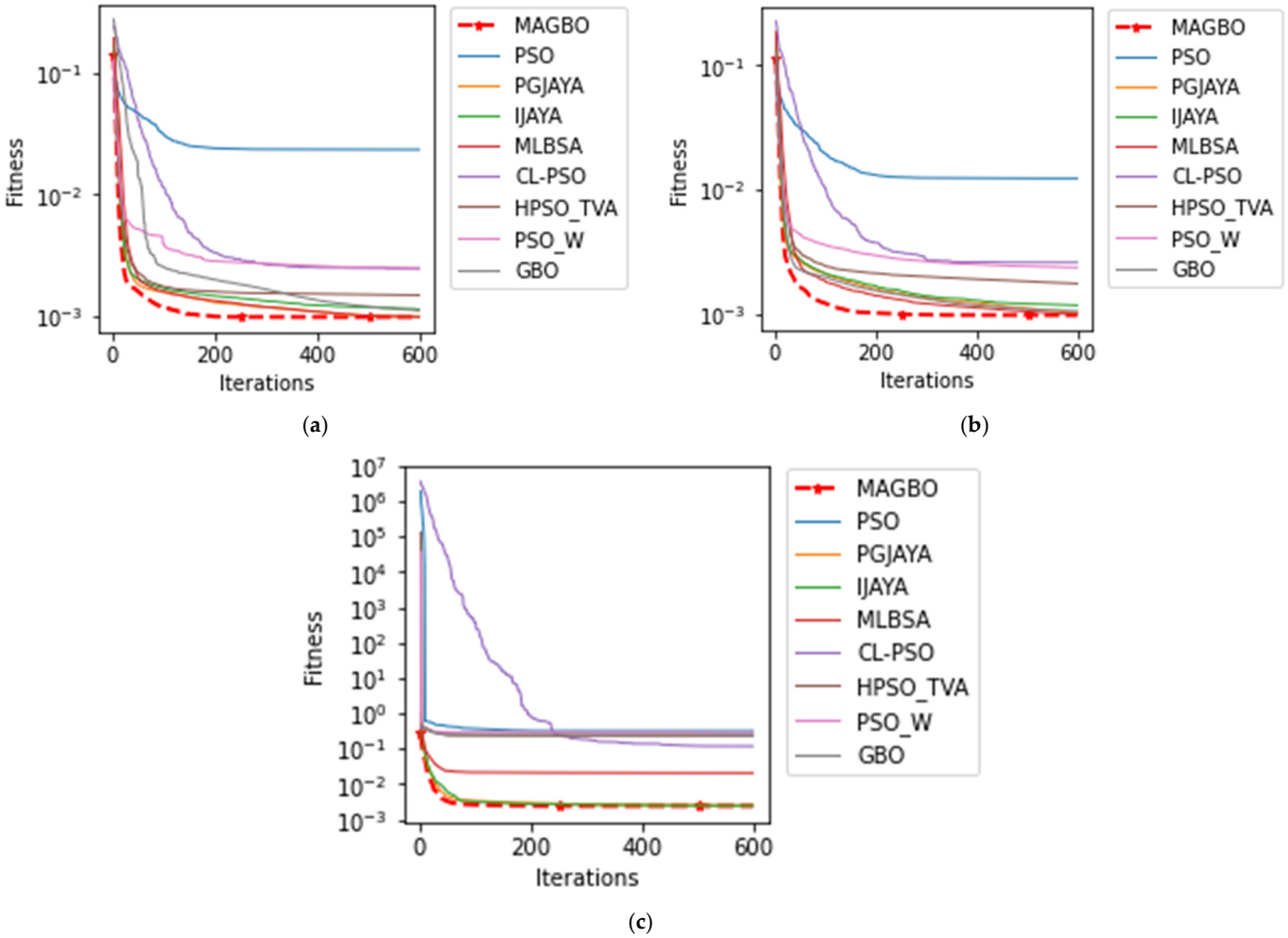

Figure 14. MAGBO and other competitors' convergence curves for three models: (**a**) Single-diode SD; (**b**) Double-diode DD; (**c**) PV module.

5.4.1. Results Obtained Using the STM6-40/36 Simulation Model

In order to evaluate how well the proposed method compares to preexisting algorithms, we publish the results from the STM6-40/36 model [86]. Figure 15 shows that the I-V and P-V curves generated by the simulation and the observations are highly consistent with one another. This supports the idea that MAGBO's projections about the STM6-40/36 model's characteristics are accurate. The STM6-40/36 model's IAE and RE are also depicted in Figure 16. The complete experimental results, including current, power, and corresponding IAR and RE values, are shown in Table 14. It was found that IAE is less than 6.08803600 $\times 10^{-3}$, which verifies that MAGBO's determination of the STM6-40/36 model's parameters is accurate. Table 15 displays the best RMSE values for each of the seven approaches and the five most significant extracted parameter values based on a total of 30 tests. Table 15 provides the RMSE values that are the most accurate, in addition to the five extracted parameter values that are the most significant, for each of the seven methods evaluated using a total of 30 tests. Table 15 shows that MAGBO produces the best results with an RMSE value of 1.72981457 $\times 10^{-3}$, the lowest possible value. Compared to other methods, the proposed MAGBO method is superior in terms of its performance when estimating the parameters of the STM6-40/36 model.

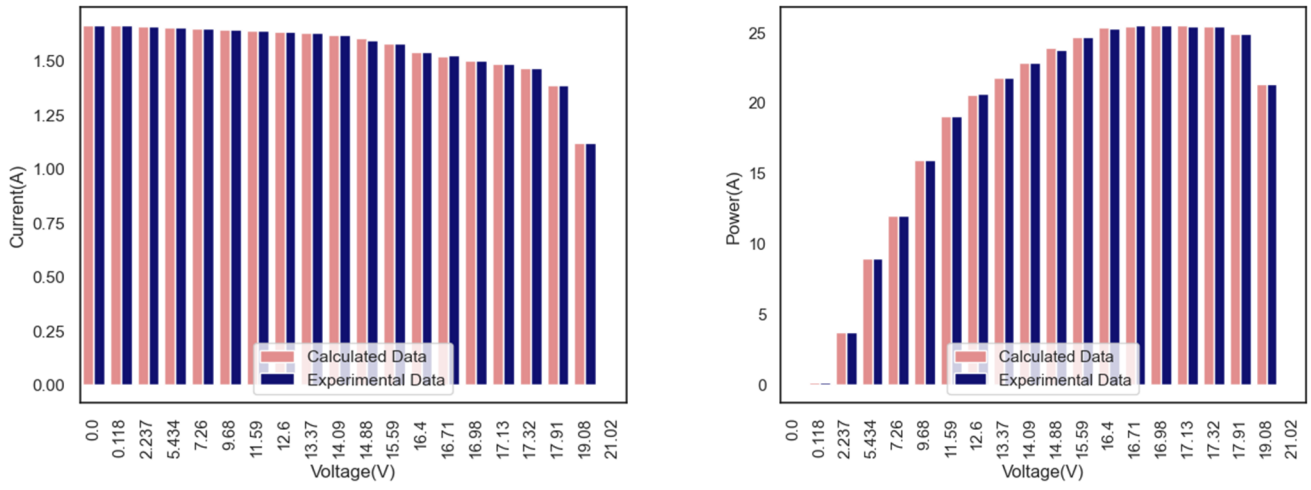

(**a**) (**b**)

Figure 15. Experimental and simulated current-voltage I–V (**a**) and power-voltage (P–V) characteristics (**b**) for an STM6-40/36 model by MAGBO.

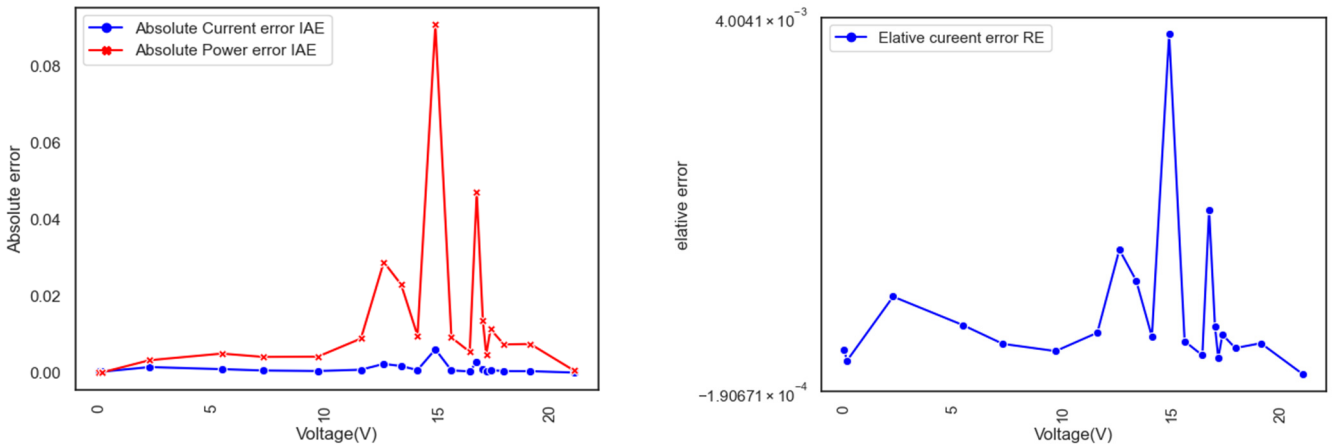

(**a**) (**b**)

Figure 16. Experimental and simulated current data error-index values of an STM6-40/36 model: (**a**) IAE; (**b**) RE.

5.4.2. Results Obtained Using the PVM 752 GaAs Thin-Film Simulation Model

Using the SDM, we analyzed the suggested MAGBO technique to learn more about the characteristics of a PVM 752 GaAs thin-film cell. Tables 16 and 17 detail the experiment outcomes, such as the current, power, IAE, and RE measured values. Table 17 displays the simulated current data alongside the IAE and RE error measurements. The optimization method was found to be more challenging when applied to calculating the parameters of the PVM 752 thin-film cell than the RTC France solar cell. Table 16 shows that despite this, the MAGBO approach is effective. Table 17 displays the outcomes of different algorithms' attempts to estimate the SDM parameters, and it can be observed that MAGBO fared best, with the lowest RMSE value. Figure 17 shows the IAE and RE currents, both experimentally and as measured, for the PVM 752 thin-film cell model. Figure 18 demonstrates that the I-V and P-V curves generated by the simulation and the measurements are highly consistent with one another, proving that MAGBO's predictions for the PVM 752 thin-film model are correct.

Table 14. Absolute MAGBO error (IAE) on the STM6-40/36 model.

Item	Measured Data		Simulated Current Data		Simulated Power Data	
	$V(V)$	$I(A)$	$I_{sim}(A)$	$IAE_I(A)$	$P_{sim}(W)$	$IAE_P(W)$
1	0	1.663	1.663458258	0.000458258	0.0000000000	0.0000000000
2	0.118	1.663	1.66325231	0.00025231	0.1962637726	0.0000297726
3	2.237	1.661	1.659550809	0.001449191	3.7124151597	0.0032418403
4	5.434	1.653	1.653914699	0.000914699	8.9873724744	0.0049704744
5	7.26	1.65	1.650565914	0.000565914	11.9831085356	0.0041085356
6	9.68	1.645	1.645430605	0.000430605	15.9277682564	0.0041682564
7	11.59	1.64	1.639233537	0.000766463	18.9987166938	0.0088833062
8	12.6	1.636	1.633712696	0.002287304	20.5847799696	0.0288200304
9	13.37	1.629	1.627285808	0.001714192	21.7568112530	0.0229187470
10	14.09	1.619	1.618313576	0.000686424	22.8020382858	0.0096717142
11	14.88	1.597	1.603090045	0.006090045	23.8539798696	0.0906198696
12	15.59	1.581	1.581588376	0.000588376	24.6569627818	0.0091727818
13	16.4	1.542	1.542330591	0.000330591	25.2942216924	0.0054216924
14	16.71	1.524	1.521192634	0.002807366	25.4191289141	0.0469110859
15	16.98	1.5	1.499194744	0.000805256	25.4563267531	0.0136732469
16	17.13	1.485	1.48527527	0.00027527	25.4427653751	0.0047153751
17	17.32	1.465	1.465654242	0.000654242	25.3851314714	0.0113314714
18	17.91	1.388	1.387589368	0.000410632	24.8517255809	0.0073544191
19	19.08	1.118	1.118391376	0.000391376	21.3389074541	0.0074674541
20	21.02	0	−0.000024814	0.000024814	−0.0005215903	0.0005215903

Table 15. A comparison of a variety of algorithms applied to the model of an STM6-40/36.

Algorithm	$I_{ph}(A)$	$I_{sd}(\mu A)$	$R_s(\Omega)$	$R_{sh}(\Omega)$	n	RMSE
MAGBO	**1.6639078**	$\mathbf{1.73865682\times10^{-6}}$	$\mathbf{1.53855769\times10^{-1}}$	$\mathbf{5.73418580\times10^{2}}$	$\mathbf{5.57630767\times10}$	$\mathbf{1.72981457\times10^{-3}}$
SEDE	1.66390478	$1.73865696 \times 10^{-6}$	$1.53855761 \times 10^{-1}$	5.73418588×10^{2}	5.57630770×10	$1.72981371 \times 10^{-3}$
MLBSA	1.66390478	$1.73865694 \times 10^{-6}$	$1.53855762 \times 10^{-1}$	5.73418594×10^{2}	5.57630770×10	$1.72981371 \times 10^{-3}$
IJAYA	1.66820359	$2.71000974 \times 10^{-7}$	$3.53241396 \times 10^{-1}$	3.85497843×10^{2}	4.91485938×10	$4.69534212 \times 10^{-3}$
JADE	1.66390478	$1.73870000 \times 10^{-6}$	$4.27377120 \times 10^{-3}$	1.59282939×10	1.52030292	$1.72981371 \times 10^{-3}$
PGJAYA	1.66390506	$1.73854219 \times 10^{-6}$	$1.53863151 \times 10^{-1}$	5.73403658×10^{2}	5.57628110×10	$1.72981372 \times 10^{-3}$
SSA	1.86482388	$3.13491034 \times 10^{-7}$	$1.35532499 \times 10^{-1}$	3.31630801×10	5.11425353×10	$1.78578316 \times 10^{-1}$
MFO	1.86239751	0.00000000	0.00000000	3.28634387×10	2.70424691×10	$3.10757409 \times 10^{-1}$
LNMHGS [87]	1.66345338	$2.08416563 \times 10^{-6}$	$1.32775299 \times 10^{-1}$	6.08102259×10^{2}	5.65036041×10	$1.78155207 \times 10^{-3}$
HSOA [85]	1.66298248	$2.51123031 \times 10^{-6}$	$1.10621018 \times 10^{-1}$	6.49583949×10^{2}	5.72859543×10	$1.93518826 \times 10^{-3}$

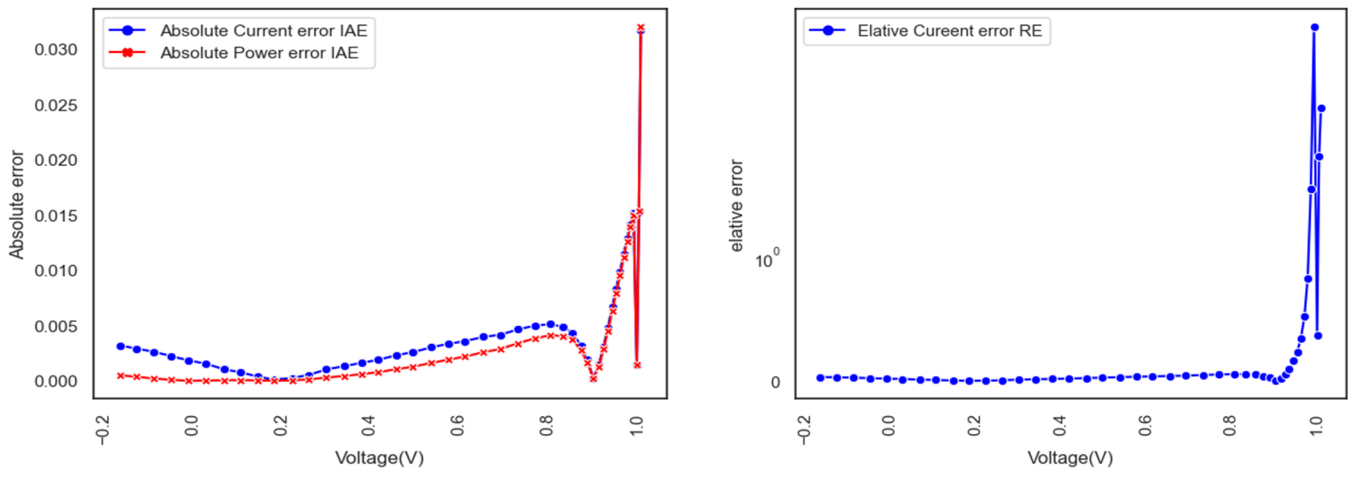

(**a**) (**b**)

Figure 17. Experimental and simulated current data error-index values of a PVM 752 GaAs thin-film model: (**a**) IAE; (**b**) RE.

Table 16. Absolute MAGBO error (IAE) on the PVM 752 GaAs thin-film model.

Item	Measured Data		Simulated Current Data		Simulated Power Data	
	$V(V)$	$I(A)$	$I_{sim}(A)$	$IAE_I(A)$	$P_{sim}(W)$	$IAE_P(W)$
1	−0.1659	0.1001	0.103313	0.003213	−0.01661	0.00053298
2	−0.1281	0.1000	0.102935	0.002935	−0.01281	0.00037599
3	−0.0888	0.0999	0.102543	0.002643	−0.00887	0.00023467
4	−0.0490	0.0999	0.102145	0.002245	−0.0049	0.00010999
5	−0.0102	0.0999	0.101757	0.001857	−0.00102	0.00001894
6	0.0275	0.0998	0.10138	0.00158	0.002745	0.00004345
7	0.0695	0.0999	0.10096	0.00106	0.006943	0.00007364
8	0.1061	0.0998	0.100594	0.000794	0.010589	0.00008426
9	0.1460	0.0998	0.100195	0.000395	0.014571	0.00005769
10	0.1828	0.0997	0.099828	0.000128	0.018225	0.00002332
11	0.2230	0.0997	0.099426	0.000274	0.022233	0.00006120
12	0.2600	0.0996	0.099056	0.000544	0.025896	0.00014145
13	0.3001	0.0997	0.098654	0.001046	0.02992	0.00031383
14	0.3406	0.0996	0.098249	0.001351	0.033924	0.00046004
15	0.3789	0.0995	0.097866	0.001634	0.037701	0.00061913
16	0.4168	0.0994	0.097486	0.001914	0.04143	0.00079786
17	0.4583	0.0994	0.097067	0.002333	0.045555	0.00106936
18	0.4949	0.0993	0.096694	0.002606	0.049144	0.00128985
19	0.5370	0.0993	0.096255	0.003045	0.053324	0.00163542
20	0.5753	0.0992	0.095837	0.003363	0.05707	0.00193487
21	0.6123	0.0990	0.095399	0.003601	0.060618	0.00220516
22	0.6546	0.0988	0.094808	0.003992	0.064674	0.00261315
23	0.6918	0.0983	0.094128	0.004172	0.068004	0.00288618
24	0.7318	0.0977	0.093039	0.004661	0.071497	0.00341085
25	0.7702	0.0963	0.091297	0.005003	0.07417	0.00385325
26	0.8053	0.0937	0.088559	0.005141	0.075457	0.00413981
27	0.8329	0.0900	0.08511	0.00489	0.074961	0.00407271
28	0.8550	0.0855	0.081137	0.004363	0.073103	0.00373058
29	0.8738	0.0799	0.076712	0.003188	0.069817	0.00278586
30	0.8887	0.0743	0.072388	0.001912	0.06603	0.00169898
31	0.9016	0.0683	0.068057	0.000243	0.061579	0.00021924
32	0.9141	0.0618	0.063224	0.001424	0.056491	0.00130153
33	0.9248	0.0555	0.058613	0.003113	0.051326	0.00287915
34	0.9344	0.0493	0.054089	0.004789	0.046066	0.00447473
35	0.9445	0.0422	0.048938	0.006738	0.039858	0.00636414
36	0.9533	0.0357	0.044051	0.008351	0.034033	0.00796108
37	0.9618	0.0291	0.038987	0.009887	0.027988	0.00950938
38	0.9702	0.0222	0.033685	0.011485	0.021538	0.01114278
39	0.9778	0.0157	0.028601	0.012901	0.015351	0.01261445
40	0.9852	0.0092	0.023347	0.014147	0.009064	0.01393780
41	0.9926	0.0026	0.017738	0.015138	0.002581	0.01502608
42	0.9999	0.0040	0.005465	0.001465	0.004	0.00146486
43	1.0046	0.0085	0.00681	0.015307	0.008539	0.01537696
44	1.0089	0.0124	0.0193	0.031703	0.01251	0.03198466

Table 17. A comparison of various algorithms applied on the model of a PVM 752 GaAs thin-film.

Algorithm	$I_{ph}(A)$	$I_{sd}(\mu A)$	$R_s(\Omega)$	$R_{sh}(\Omega)$	n	RMSE
MAGBO	$\mathbf{1.021541340\times10^{-1}}$	$\mathbf{4.912951570\times10^{-10}}$	$\mathbf{5.000000000\times10^{-1}}$	$\mathbf{1.000000000\times10^{2}}$	**2.000000000**	$\mathbf{7.498895770\times10^{-3}}$
SEDE	1.021541340×10^{-1}	$4.912951570\times10^{-10}$	5.000000000×10^{-1}	1.000000000×10^{2}	2.000000000	7.498895770×10^{-3}
MLBSA	1.021541340×10^{-1}	$4.912951570\times10^{-10}$	5.000000000×10^{-1}	1.000000000×10^{2}	2.000000000	7.498928370×10^{-3}
IJAYA	1.021541340×10^{-1}	$4.912951570\times10^{-10}$	5.000000000×10^{-1}	1.000000000×10^{2}	2.000000000	7.498895770×10^{-3}
JADE	1.021541340×10^{-1}	$4.912951570\times10^{-10}$	5.000000000×10^{-1}	1.000000000×10^{2}	2.000000000	7.498895770×10^{-3}
PGJAYA	1.021541340×10^{-1}	$4.912951560\times10^{-10}$	5.000000000×10^{-1}	1.000000000×10^{2}	2.000000000	7.498895770×10^{-3}
SSA	1.025574810×10^{-1}	$3.993709460\times10^{-10}$	1.706274330×10^{-2}	6.503079280×10	1.972598610	9.017017310×10^{-3}
MFO	1.021541340×10^{-1}	$4.912951570\times10^{-10}$	5.000000000×10^{-1}	1.000000000×10^{2}	2.000000000	7.498895770×10^{-3}
LNMHGS [87]	1.021541340×10^{-1}	$4.912951560\times10^{-10}$	5.000000000×10^{-1}	1.000000000×10^{2}	2.000000000	7.498895770×10^{-3}
HSOA [85]	1.021541340×10^{-1}	$4.912951570\times10^{-10}$	5.000000000×10^{-1}	1.000000000×10^{2}	2.000000000	7.498895770×10^{-3}

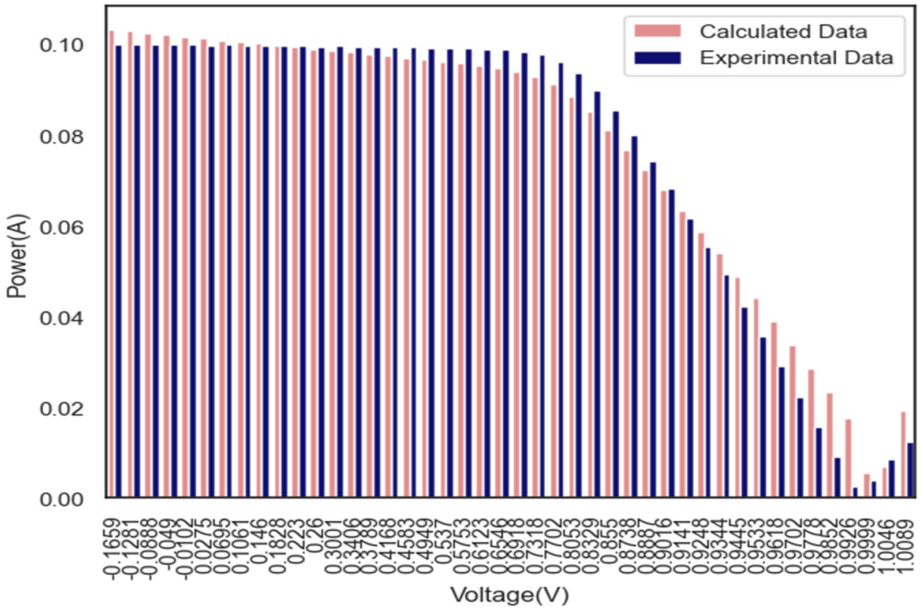

(**a**)

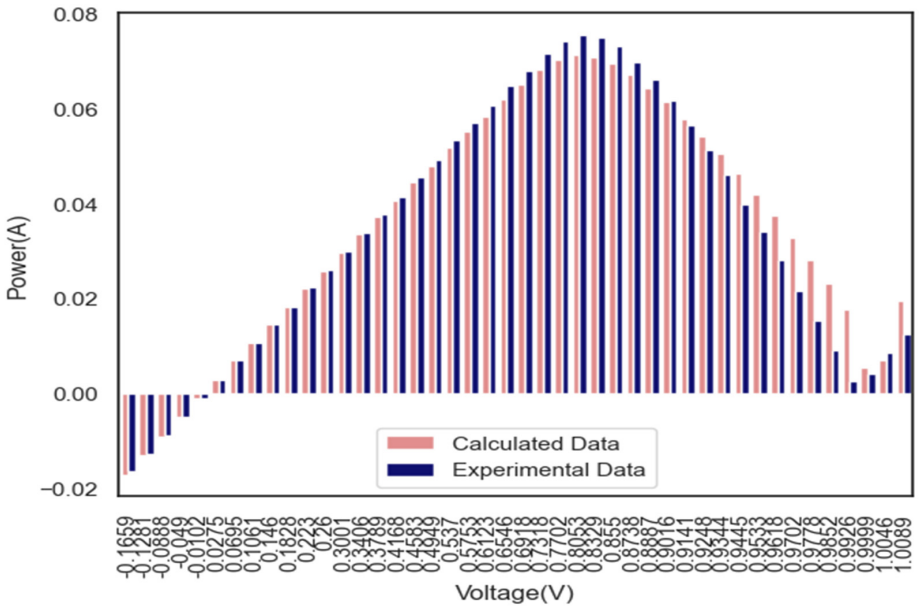

(**b**)

Figure 18. Experimental and simulated current-voltage I–V (**a**) and power–voltage (P–V) characteristics (**b**) for PVM 752 GaAs thin-film model by MAGBO.

6. Problem Limitation

Even if it performs better than certain other algorithms already on the market for the chosen tests, MAGBO has a few drawbacks. The following are some of our ideas regarding the primary restrictions imposed by the algorithm: to begin, the research does not address a large-scale optimization problem that involves more than 500 choice variables related to scalability. Second, the suggested method can successfully obtain optimal global solutions and is utilized to optimize the process of extracting parameters from static models of solar photovoltaic systems. In addition, the report completely ignores the difficulties associated with the dynamic model. Finally, while selecting multi-objective real-world issues, it is a good idea to consider a mix of computing time, complexity, stability, and scalability. This is because these factors all play a role in the solution.

7. Conclusions and Future Work

Solar energy is one of the most important forms of renewable energy that has the potential to replace fossil fuels. Unlike fossil fuels, solar energy does not release any harmful gaseous emissions that are a major factor in the degradation of the natural environment and a consequent risk to the well-being of all forms of life. The vital activity of parameter extraction is a component of the optimization process for solar power systems. In this research, optimal solutions can be discovered by utilizing a more recent and improved algorithm known as MAGBO. The modified gradient search rule (MGSR), which was derived from the quasi-Newton method to improve its local and global capabilities, a new refresh operator (NRO), which was designed to improve solution quality and algorithm exploration abilities, and a crossover mechanism, which was designed to balance exploitation and boost the population's variety, were all combined by MAGBO to create a novel approach that overcomes the shortcomings of the standard GBO. A precise evaluation of MAGBO's usefulness was made possible thanks to the successful extraction of parameters from various PV models, such as single and double-diode (DDM), PV modules, as well as the CEC2021 test suite. The results revealed that the recently developed MAGBO algorithm performed better than its contemporaries, including the first version of the GBO algorithm. According to the findings, MAGBO can compete with numerous other algorithms already in use, establishing it as a viable alternative approach for determining the parameters of solar models. Further study will present additional strategies to complement the suggested algorithm to address other energy-related optimization difficulties, particularly the dynamic models. This will be done to improve the overall quality of the proposed solution. In addition, the technique that has been described can be utilized to address large-scale global optimization issues without compromising diversity. In addition, MAGBO has not been considered from a medical point of view at any step in this process. As a direct consequence, the MAGBO that has been proposed will conduct an experiment on this subject.

Author Contributions: Conceptualization, M.Q. and N.K.H.; methodology, M.Q. and B.S.M.; software, M.Q. and M.A.; validation, M.A., M.Q. and N.K.H.; formal analysis, M.A.; investigation, B.S.M. and M.A.; resources, M.A.; data curation, B.S.M., M.A. and M.Q.; writing—original draft preparation, N.K.H.; writing—review and editing, M.Q., B.S.M., M.A. and N.K.H.; visualization, M.Q., B.S.M., M.A. and N.K.H.; supervision, M.Q., B.S.M., M.A. and N.K.H.; project administration, M.Q. and N.K.H. All authors have read and agreed to the published version of the manuscript.

Funding: This research was funded by the Deputyship for Research & Innovation, Ministry of Education in Saudi Arabia, project number 445-9-394.

Data Availability Statement: We have made the code for this research project available on GitHub. at https://github.com/MohammedQaraad/MAGBO-algorithm, (accessed on 22 September 2023). Readers interested in accessing the code can download it from this repository.

Acknowledgments: The authors extend their appreciation to the Deputyship for Research and Innovation, Ministry of Education in Saudi Arabia, for funding this research work through project number 445-9-394.

Conflicts of Interest: The authors declare no conflict of interest.

References

1. Mcelroy, M.B.; Chen, X. Wind and Solar Power in the United States: Status and Prospects. *CSEE J. Power Energy Syst.* **2017**, *3*, 1–6. [CrossRef]
2. Alam, D.F.; Yousri, D.A.; Eteiba, M.B. Flower Pollination Algorithm Based Solar PV Parameter Estimation. *Energy Convers. Manag.* **2015**, *101*, 410–422. [CrossRef]
3. Fathy, A.; Rezk, H. Parameter Estimation of Photovoltaic System Using Imperialist Competitive Algorithm. *Renew. Energy* **2017**, *111*, 307–320. [CrossRef]
4. Chin, V.J.; Salam, Z.; Ishaque, K. Cell Modelling and Model Parameters Estimation Techniques for Photovoltaic Simulator Application: A Review. *Appl. Energy* **2015**, *154*, 500–519. [CrossRef]
5. Batzelis, E.I.; Papathanassiou, S.A. A Method for the Analytical Extraction of the Single-Diode PV Model Parameters. *IEEE Trans. Sustain. Energy* **2015**, *7*, 504–512.

6. Louzazni, M.; Aroudam, E.H. An Analytical Mathematical Modeling to Extract the Parameters of Solar Cell from Implicit Equation to Explicit Form. *Appl. Sol. Energy* **2015**, *51*, 165–171.
7. Brano, V.L.; Ciulla, G. An Efficient Analytical Approach for Obtaining a Five Parameters Model of Photovoltaic Modules Using Only Reference Data. *Appl. Energy* **2013**, *111*, 894–903.
8. Stornelli, V.; Muttillo, M.; De Rubeis, T.; Nardi, I. A New Simplified Five-Parameter Estimation Method for Single-Diode Model of Photovoltaic Panels. *Energies* **2019**, *12*, 4271.
9. Atay, B.K.; Eminoğlu, U. A New Approach for Parameter Estimation of the Single-Diode Model Forphotovoltaic Cells/Modules. *Turkish J. Electr. Eng. Comput. Sci.* **2019**, *27*, 3026–3039. [CrossRef]
10. Qaraad, M.; Amjad, S.; Hussein, N.K.; Elhosseini, M.A. Addressing Constrained Engineering Problems and Feature Selection with a Time-Based Leadership Salp-Based Algorithm with Competitive Learning. *J. Comput. Des. Eng.* **2022**, *9*, 2235–2270.
11. Mehta, H.K.; Warke, H.; Kukadiya, K.; Panchal, A.K. Accurate Expressions for Single-Diode-Model Solar Cell Parameterization. *IEEE J. Photovolt.* **2019**, *9*, 803–810.
12. Lun, S.; Du, C.; Guo, T.; Wang, S.; Sang, J.; Li, J. A New Explicit I–V Model of a Solar Cell Based on Taylor's Series Expansion. *Sol. Energy* **2013**, *94*, 221–232.
13. Easwarakhanthan, T.; Bottin, J.; Bouhouch, I.; Boutrit, C. Nonlinear Minimization Algorithm for Determining the Solar Cell Parameters with Microcomputers. *Int. J. Sol. Energy* **1986**, *4*, 1–12. [CrossRef]
14. Cabestany, J.; Castaner, L. Evaluation of Solar Cell Parameters by Nonlinear Algorithms. *J. Phys. D Appl. Phys.* **1983**, *16*, 2547. [CrossRef]
15. Li, S.; Gong, W.; Gu, Q. A Comprehensive Survey on Meta-Heuristic Algorithms for Parameter Extraction of Photovoltaic Models. *Renew. Sustain. Energy Rev.* **2021**, *141*, 110828. [CrossRef]
16. Ismail, M.S.; Moghavvemi, M.; Mahlia, T.M.I. Characterization of PV Panel and Global Optimization of Its Model Parameters Using Genetic Algorithm. *Energy Convers. Manag.* **2013**, *73*, 10–25.
17. Ahmadianfar, I.; Bozorg-Haddad, O.; Chu, X. Gradient-Based Optimizer: A New Metaheuristic Optimization Algorithm. *Inf. Sci.* **2020**, *540*, 131–159. [CrossRef]
18. Hamid, N.F.A.; Rahim, N.A.; Selvaraj, J. Solar Cell Parameters Extraction Using Particle Swarm Optimization Algorithm. In Proceedings of the 2013 IEEE Conference on Clean Energy and Technology (CEAT), Langkawi, Malaysia, 18–20 November 2013; pp. 461–465.
19. El-Naggar, K.M.; AlRashidi, M.R.; AlHajri, M.F.; Al-Othman, A.K. Simulated Annealing Algorithm for Photovoltaic Parameters Identification. *Sol. Energy* **2012**, *86*, 266–274.
20. Oliva, D.; Cuevas, E.; Pajares, G. Parameter Identification of Solar Cells Using Artificial Bee Colony Optimization. *Energy* **2014**, *72*, 93–102. [CrossRef]
21. Yuan, X.; He, Y.; Liu, L. Parameter Extraction of Solar Cell Models Using Chaotic Asexual Reproduction Optimization. *Neural Comput. Appl.* **2015**, *26*, 1227–1239.
22. Yu, K.; Liang, J.J.; Qu, B.Y.; Cheng, Z.; Wang, H. Multiple Learning Backtracking Search Algorithm for Estimating Parameters of Photovoltaic Models. *Appl. Energy* **2018**, *226*, 408–422. [CrossRef]
23. Kang, T.; Yao, J.; Jin, M.; Yang, S.; Duong, T. A Novel Improved Cuckoo Search Algorithm for Parameter Estimation of Photovoltaic (PV) Models. *Energies* **2018**, *11*, 1060.
24. Niu, Q.; Zhang, L.; Li, K. A Biogeography-Based Optimization Algorithm with Mutation Strategies for Model Parameter Estimation of Solar and Fuel Cells. *Energy Convers. Manag.* **2014**, *86*, 1173–1185. [CrossRef]
25. Wang, G.G.; Deb, S.; Cui, Z. Monarch Butterfly Optimization. *Neural Comput. Appl.* **2015**, *31*, 1995–2014. [CrossRef]
26. Qais, M.H.; Hasanien, H.M.; Alghuwainem, S. Identification of Electrical Parameters for Three-Diode Photovoltaic Model Using Analytical and Sunflower Optimization Algorithm. *Appl. Energy* **2019**, *250*, 109–117.
27. Qais, M.H.; Hasanien, H.M.; Alghuwainem, S.; Nouh, A.S. Coyote Optimization Algorithm for Parameters Extraction of Three-Diode Photovoltaic Models of Photovoltaic Modules. *Energy* **2019**, *187*, 116001.
28. Subudhi, B.; Pradhan, R. Bacterial Foraging Optimization Approach to Parameter Extraction of a Photovoltaic Module. *IEEE Trans. Sustain. Energy* **2017**, *9*, 381–389. [CrossRef]
29. Chen, H.; Jiao, S.; Wang, M.; Heidari, A.A.; Zhao, X. Parameters Identification of Photovoltaic Cells and Modules Using Diversification-Enriched Harris Hawks Optimization with Chaotic Drifts. *J. Clean. Prod.* **2020**, *244*, 118778.
30. Benkercha, R.; Moulahoum, S.; Taghezouit, B. Extraction of the PV Modules Parameters with MPP Estimation Using the Modified Flower Algorithm. *Renew. Energy* **2019**, *143*, 1698–1709.
31. Houssein, E.H.; Zaki, G.N.; Abualigah, L.; Younis, E.M.G. Metaheuristics for Parameter Estimation of Solar Photovoltaic Cells: A Comprehensive Review. *Stud. Comput. Intell.* **2022**, *1038*, 149–179.
32. Ridha, H.M.; Hizam, H.; Mirjalili, S.; Othman, M.L.; Ya'acob, M.E.; Ahmadipour, M. Parameter Extraction of Single, Double, and Three Diodes Photovoltaic Model Based on Guaranteed Convergence Arithmetic Optimization Algorithm and Modified Third Order Newton Raphson Methods. *Renew. Sustain. Energy Rev.* **2022**, *162*, 112436. [CrossRef]
33. Wolpert, D.H.; Macready, W.G. No Free Lunch Theorems for Optimization. *IEEE Trans. Evol. Comput.* **1997**, *1*, 67–82. [CrossRef]
34. Aliramezani, M.; Koch, C.R.; Shahbakhti, M. *Modeling, Diagnostics, Optimization, and Control of Internal Combustion Engines via Modern Machine Learning Techniques: A Review and Future Directions*; Elsevier: Amsterdam, The Netherlands, 2022. [CrossRef]
35. Baburaj, E. Comparative Analysis of Bio-Inspired Optimization Algorithms in Neural Network-Based Data Mining Classification. *Int. J. Swarm Intell. Res. (IJSIR)* **2022**, *13*, 1–25.

36. Brookes, D.H.; Aghazadeh, A.; Listgarten, J. On the Sparsity of Fitness Functions and Implications for Learning. *Proc. Natl. Acad. Sci. USA* **2022**, *119*, e2109649118. [CrossRef]
37. Deng, W.; Shang, S.; Cai, X.; Zhao, H.; Zhou, Y.; Chen, H.; Deng, W. *Quantum Differential Evolution with Cooperative Coevolution Framework and Hybrid Mutation Strategy for Large Scale Optimization*; Elsevier: Amsterdam, The Netherlands, 2021.
38. LaTorre, A.; Molina, D.; Osaba, E.; Poyatos, J.; Del Ser, J.; Herrera, F. *A Prescription of Methodological Guidelines for Comparing Bio-Inspired Optimization Algorithms*; Elsevier: Amsterdam, The Netherlands, 2021.
39. Deng, W.; Zhang, X.; Zhou, Y.; Liu, Y.; Zhou, X.; Chen, H.; Zhao, H. *An Enhanced Fast Non-Dominated Solution Sorting Genetic Algorithm for Multi-Objective Problems*; Elsevier: Amsterdam, The Netherlands, 2022.
40. Wu, E.Q.; Zhou, M.; Hu, D.; Zhu, L.; Tang, Z.; Qiu, X.Y.; Deng, P.Y.; Zhu, L.M.; Ren, H. Self-Paced Dynamic Infinite Mixture Model for Fatigue Evaluation of Pilots' Brains. *IEEE Trans. Cybern.* **2020**, *52*, 5623–5638.
41. Mirjalili, S. Moth-Flame Optimization Algorithm: A Novel Nature-Inspired Heuristic Paradigm. *Knowl.-Based Syst.* **2015**, *89*, 228–249. [CrossRef]
42. Li, M.D.; Zhao, H.; Weng, X.W.; Han, T. A Novel Nature-Inspired Algorithm for Optimization: Virus Colony Search. *Adv. Eng. Softw.* **2016**, *165*, 1339–1351. [CrossRef]
43. Hashim, F.A.; Houssein, E.H.; Mabrouk, M.S.; Al-Atabany, W.; Mirjalili, S. Henry Gas Solubility Optimization: A Novel Physics-Based Algorithm. *Futur. Gener. Comput. Syst.* **2019**, *101*, 646–667. [CrossRef]
44. Qaraad, M.; Aljadania, A.; Elhosseini, M. Large-Scale Competitive Learning-Based Salp Swarm for Global Optimization and Solving Constrained Mechanical and Engineering Design Problems. *Mathematics* **2023**, *11*, 1362. [CrossRef]
45. Yu, K.; Qu, B.; Yue, C.; Ge, S.; Chen, X.; Liang, J. A Performance-Guided JAYA Algorithm for Parameters Identification of Photovoltaic Cell and Module. *Appl. Energy* **2019**, *237*, 241–257. [CrossRef]
46. Nadimi-Shahraki, M.H.; Taghian, S.; Mirjalili, S. An Improved Grey Wolf Optimizer for Solving Engineering Problems. *Expert Syst. Appl.* **2021**, *166*, 113917. [CrossRef]
47. Nadimi-Shahraki, M.H.; Taghian, S.; Mirjalili, S.; Faris, H. MTDE: An Effective Multi-Trial Vector-Based Differential Evolution Algorithm and Its Applications for Engineering Design Problems. *Appl. Soft Comput.* **2020**, *97*, 106761. [CrossRef]
48. Nadimi-Shahraki, M.H.; Taghian, S.; Zamani, H.; Mirjalili, S.; Elaziz, M.A. MMKE: Multi-Trial Vector-Based Monkey King Evolution Algorithm and Its Applications for Engineering Optimization Problems. *PLoS ONE* **2023**, *18*, e0280006. [CrossRef]
49. Nadimi-Shahraki, M.H.; Taghian, S.; Mirjalili, S.; Abualigah, L. Binary Aquila Optimizer for Selecting Effective Features from Medical Data: A COVID-19 Case Study. *Mathematics* **2022**, *10*, 1929. [CrossRef]
50. Nadimi-Shahraki, M.H.; Moeini, E.; Taghian, S.; Mirjalili, S. DMFO-CD: A Discrete Moth-Flame Optimization Algorithm for Community Detection. *Algorithms* **2021**, *14*, 314. [CrossRef]
51. Daoud, M.S.; Shehab, M.; Al-Mimi, H.M.; Abualigah, L.; Zitar, R.A.; Shambour, M.K.Y. Gradient-Based Optimizer (GBO): A Review, Theory, Variants, and Applications. *Arch. Comput. Methods Eng.* **2022**, *1*, 1–19.
52. Alorf, A. A Survey of Recently Developed Metaheuristics and Their Comparative Analysis. *Eng. Appl. Artif. Intell.* **2023**, *117*, 105622. [CrossRef]
53. Yu, K.; Liang, J.J.; Qu, B.Y.; Chen, X.; Wang, H. Parameters Identification of Photovoltaic Models Using an Improved JAYA Optimization Algorithm. *Energy Convers. Manag.* **2017**, *150*, 742–753. [CrossRef]
54. Zhang, J.; Sanderson, A.C. JADE: Adaptive Differential Evolution with Optional External Archive. *IEEE Trans. Evol. Comput.* **2009**, *13*, 945–958. [CrossRef]
55. Liang, J.; Qiao, K.; Yu, K.; Ge, S.; Qu, B.; Xu, R.; Li, K. Parameters Estimation of Solar Photovoltaic Models via a Self-Adaptive Ensemble-Based Differential Evolution. *Sol. Energy* **2020**, *207*, 336–346. [CrossRef]
56. Hassan, M.H.; Kamel, S.; El-Dabah, M.A.; Rezk, H. A Novel Solution Methodology Based on a Modified Gradient-Based Optimizer for Parameter Estimation of Photovoltaic Models. *Electronics* **2021**, *10*, 472. [CrossRef]
57. Jiang, Y.; Luo, Q.; Zhou, Y. Improved Gradient-Based Optimizer for Parameters Extraction of Photovoltaic Models. *IET Renew. Power Gener.* **2022**, *16*, 1602–1622. [CrossRef]
58. Premkumar, M.; Jangir, P.; Elavarasan, R.M.; Sowmya, R. Opposition Decided Gradient-Based Optimizer with Balance Analysis and Diversity Maintenance for Parameter Identification of Solar Photovoltaic Models. *J. Ambient Intell. Humaniz. Comput.* **2023**, *14*, 7109–7131.
59. Zhou, W.; Wang, P.; Heidari, A.A.; Zhao, X.; Turabieh, H.; Chen, H. Random Learning Gradient Based Optimization for Efficient Design of Photovoltaic Models. *Energy Convers. Manag.* **2021**, *230*, 113751. [CrossRef]
60. Yu, S.; Chen, Z.; Heidari, A.A.; Zhou, W.; Chen, H.; Xiao, L. Parameter Identification of Photovoltaic Models Using a Sine Cosine Differential Gradient Based Optimizer. *IET Renew. Power Gener.* **2022**, *16*, 1535–1561. [CrossRef]
61. Ramadan, A.; Kamel, S.; Hassan, M.H.; Tostado-Véliz, M.; Eltamaly, A.M. Parameter Estimation of Static/Dynamic Photovoltaic Models Using a Developed Version of Eagle Strategy Gradient-Based Optimizer. *Sustainability* **2021**, *13*, 13053. [CrossRef]
62. Qaraad, M.; Amjad, S.; Hussein, N.K.; Badawy, M.; Mirjalili, S.; Elhosseini, M.A. Photovoltaic Parameter Estimation Using Improved Moth Flame Algorithms with Local Escape Operators. *Comput. Electr. Eng.* **2023**, *106*, 108603. [CrossRef]
63. Özban, A.Y. Some New Variants of Newton's Method. *Appl. Math. Lett.* **2004**, *17*, 677–682. [CrossRef]
64. Liu, Y.; Chong, G.; Heidari, A.A.; Chen, H.; Liang, G.; Ye, X.; Cai, Z.; Wang, M. Horizontal and Vertical Crossover of Harris Hawk Optimizer with Nelder-Mead Simplex for Parameter Estimation of Photovoltaic Models. *Energy Convers. Manag.* **2020**, *223*, 113211.

65. Fan, Y.; Wang, P.; Heidari, A.A.; Zhao, X.; Turabieh, H.; Chen, H. Delayed Dynamic Step Shuffling Frog-Leaping Algorithm for Optimal Design of Photovoltaic Models. *Energy Rep.* **2021**, *7*, 228–246.
66. Yu, K.; Chen, X.; Wang, X.; Wang, Z. Parameters Identification of Photovoltaic Models Using Self-Adaptive Teaching-Learning-Based Optimization. *Energy Convers. Manag.* **2017**, *145*, 233–246.
67. Chen, X.; Yu, K.; Du, W.; Zhao, W.; Liu, G. Parameters Identification of Solar Cell Models Using Generalized Oppositional Teaching Learning Based Optimization. *Energy* **2016**, *99*, 170–180. [CrossRef]
68. Li, S.; Gong, W.; Yan, X.; Hu, C.; Bai, D.; Wang, L.; Gao, L. Parameter Extraction of Photovoltaic Models Using an Improved Teaching-Learning-Based Optimization. *Energy Convers. Manag.* **2019**, *186*, 293–305. [CrossRef]
69. Chen, H.; Jiao, S.; Heidari, A.A.; Wang, M.; Chen, X.; Zhao, X. An Opposition-Based Sine Cosine Approach with Local Search for Parameter Estimation of Photovoltaic Models. *Energy Convers. Manag.* **2019**, *195*, 927–942.
70. Ridha, H.M.; Gomes, C.; Hizam, H.; Ahmadipour, M.; Heidari, A.A.; Chen, H. Multi-Objective Optimization and Multi-Criteria Decision-Making Methods for Optimal Design of Standalone Photovoltaic System: A Comprehensive Review. *Renew. Sustain. Energy Rev.* **2021**, *135*, 110202.
71. Zhang, H.; Heidari, A.A.; Wang, M.; Zhang, L.; Chen, H.; Li, C. Orthogonal Nelder-Mead Moth Flame Method for Parameters Identification of Photovoltaic Modules. *Energy Convers. Manag.* **2020**, *211*, 112764.
72. Abbassi, R.; Abbassi, A.; Heidari, A.A.; Mirjalili, S. An Efficient Salp Swarm-Inspired Algorithm for Parameters Identification of Photovoltaic Cell Models. *Energy Convers. Manag.* **2019**, *179*, 362–372. [CrossRef]
73. Special Session on Real. Available online: https://www3.ntu.edu.sg/home/epnsugan/index_files/CEC2021/CEC2021-2.htm (accessed on 23 December 2022).
74. Ahmadianfar, I.; Gong, W.; Heidari, A.A.; Golilarz, N.A.; Samadi-Koucheksaraee, A.; Chen, H. Gradient-Based Optimization with Ranking Mechanisms for Parameter Identification of Photovoltaic Systems. *Energy Rep.* **2021**, *7*, 3979–3997. [CrossRef]
75. Li, S.; Chen, H.; Wang, M.; Heidari, A.A.; Mirjalili, S. Slime Mould Algorithm: A New Method for Stochastic Optimization. *Future Gener. Comput. Syst.* **2020**, *111*, 300–323. [CrossRef]
76. Kennedy, J.; Eberhart, R. Particle Swarm Optimization. In Proceedings of the ICNN'95—International Conference on Neural Networks, Perth, WA, Australia, 27 November–1 December 1995; Volume 4, pp. 1942–1948.
77. Faramarzi, A.; Heidarinejad, M.; Stephens, B.; Mirjalili, S. Equilibrium Optimizer: A Novel Optimization Algorithm. *Knowl.-Based Syst.* **2020**, *191*, 105190. [CrossRef]
78. Qin, A.K.; Huang, V.L.; Suganthan, P.N. Differential Evolution Algorithm with Strategy Adaptation for Global Numerical Optimization. *IEEE Trans. Evol. Comput.* **2009**, *13*, 398–417. [CrossRef]
79. Liang, J.J.; Qin, A.K.; Suganthan, P.N.; Baskar, S. Comprehensive Learning Particle Swarm Optimizer for Global Optimization of Multimodal Functions. *IEEE Trans. Evol. Comput.* **2006**, *10*, 281–295. [CrossRef]
80. Ghasemi, M.; Aghaei, J.; Hadipour, M. New Self-Organising Hierarchical PSO with Jumping Time-Varying Acceleration Coefficients. *Electron. Lett.* **2017**, *53*, 1360–1362. [CrossRef]
81. Bakır, H. Comparative Performance Analysis of Metaheuristic Search Algorithms in Parameter Extraction for Various Solar Cell Models. *Environ. Chall.* **2023**, *11*, 100720. [CrossRef]
82. Rezaee Jordehi, A. Enhanced Leader Particle Swarm Optimisation (ELPSO): An Efficient Algorithm for Parameter Estimation of Photovoltaic (PV) Cells and Modules. *Sol. Energy* **2018**, *159*, 78–87. [CrossRef]
83. Tong, N.T.; Pora, W. A Parameter Extraction Technique Exploiting Intrinsic Properties of Solar Cells. *Appl. Energy* **2016**, *176*, 104–115. [CrossRef]
84. Yu, S.; Heidari, A.A.; He, C.; Cai, Z.; Althobaiti, M.M.; Mansour, R.F.; Liang, G.; Chen, H. Parameter Estimation of Static Solar Photovoltaic Models Using Laplacian Nelder-Mead Hunger Games Search. *Sol. Energy* **2022**, *242*, 79–104. [CrossRef]
85. Long, W.; Jiao, J.; Liang, X.; Xu, M.; Tang, M.; Cai, S. Parameters Estimation of Photovoltaic Models Using a Novel Hybrid Seagull Optimization Algorithm. *Energy* **2022**, *249*, 123760. [CrossRef]
86. Liang, J.; Qiao, K.; Yu, K.; Qu, B.; Yue, C.; Guo, W.; Wang, L. Utilizing the Relationship Between Unconstrained and Constrained Pareto Fronts for Constrained Multiobjective Optimization. *IEEE Trans. Cybern.* **2023**, *53*, 3873–3886. [CrossRef]
87. Yu, K.; Zhang, D.; Liang, J.; Chen, K.; Yue, C.; Qiao, K.; Wang, L. A Correlation-Guided Layered Prediction Approach for Evolutionary Dynamic Multiobjective Optimization. *IEEE Trans. Evol. Comput.* **2022**. [CrossRef]